Uncrewed aerial vehicle-based assessments of peatland permafrost vulnerability along the Labrador Sea coastline, northern Canada

Jordan Beer, M.Sc., [1] **Yifeng Wang, M.Sc.,** [2] **Robert Way, Ph.D.,** [3] **Anika Forget, M.Sc.,** [4] **Victoria Colyn, B.Sc.** [5]

[1]Northern Environmental Geoscience Laboratory, Queen's University, Kingston, Ontario. E-mail: jordan.beer@queensu.ca
[2]Northern Environmental Geoscience Laboratory, Queen's University, Kingston, Ontario. E-mail: yifeng.wang@queensu.ca
[3]Northern Environmental Geoscience Laboratory, Queen's University, Kingston, Ontario. E-mail: robert.way@queensu.ca
[4]Northern Environmental Geoscience Laboratory, Queen's University, Kingston, Ontario. E-mail: anika.forget@queensu.ca
[5]Northern Environmental Geoscience Laboratory, Queen's University, Kingston, Ontario. E-mail: victoria.colyn@queensu.ca

This manuscript has undergone one round of peer-review at Permafrost and Periglacial Processes, and is currently pending further review. Please feel free to contact the corresponding author with any questions or feedback.

Abstract

Palsas and peat plateaus in subarctic peatlands are some of the southernmost lowland permafrost landforms in the Northern Hemisphere. Peatland permafrost along the Labrador Sea coastline in northeastern Canada has remained largely understudied and uncharacterised, despite the importance of these landforms for wildlife, carbon stores, and Indigenous land users. In this study, we derived geomorphological and resiliency indices for peatland permafrost landforms at 20 wetland complexes, spanning a latitudinal gradient from Blanc-Sablon, QC (51.4°N) to Nain, NL (56.5°N). Orthomosaics and three-dimensional point clouds were created for each site using high-resolution UAV-based surveys and structure-from-motion photogrammetry. Analyses revealed that peatland permafrost landforms along the Labrador Sea coastline are characterised by short heights (maximum height: 3.65 m, average height: 0.49 m), with lichen and dwarf shrub cover, making them more similar to features in northern Europe than western Canada. Palsas and peat plateaus ranged in size from 49 m^2 to 14,233 m^2, with a median feature size of 259 m^2 across all sites. Peatland permafrost in the region exhibits high levels of fragmentation, with most study sites (90%) exhibiting low or very low thaw resiliency. Results from this study indicate that peatland permafrost in many parts of Labrador are vulnerable to degradational processes with potential negative consequences for species with high cultural value to Labrador Inuit and Innu.

Keywords: permafrost, peatland, Labrador, UAV, resiliency

Introduction

Permafrost is rapidly thawing across the circumpolar North because of climate and ecosystem change (Grant et al., 2019; Mamet et al., 2017; Smith et al., 2022). Thawing permafrost and melting ground ice often lead to shifts in hydrology, vegetation, wildlife habitat, nutrient cycling, and greenhouse gas exchanges (Baltzer et al., 2014; Carpino et al., 2021; Disher et al., 2021). Permafrost thaw can also exacerbate climatic warming by releasing methane stored in previously frozen organic material (Schuur et al., 2015; Tarnocai et al., 2009). Discontinuous permafrost is amongst the most vulnerable to thaw, with many of these landscapes drastically changing in recent decades (Chasmer & Hopkinson, 2017; Holloway & Lewkowicz, 2020; James et al., 2013; Payette et al., 2004). These shifts can impact Indigenous land users who continue to harvest plant and wildlife species throughout northern Canada (Anderson et al., 2018; Dyke & Sladen, 2010; Norton et al; 2021; Ward et al., 2021).

At its southern limit, lowland permafrost is typically found in wetlands, where the insulating properties of dry peat prevents the ground from thawing in warm summer months (Smith & Riseborough, 2002). Permafrost in these environments is found within raised landforms known as palsas and peat plateaus. These features initially form when wind-driven snow redistribution promotes localised areas of deeper freezing, facilitating areas that remain frozen in summer (Seppälä, 2011). Water accumulates at the permafrost's basal freezing front during warmer months through the process of cryosuction (Hohmann, 1997). In winter, this water freezes to form layers of ice (i.e., ice lenses) that force the ground surface upwards through the process of frost heave (Peppin & Style, 2013). This iterative process ultimately creates raised mounds (palsas and/or peat plateaus) within a peatland.

While it is generally understood that palsas and peat plateaus follow similar patterns of initial development, the two landforms differ in their morphology. Palsas typically form dome-shaped mounds that can vary in height from just a few centimetres up to 10 metres and exist as individual "islands" in the peatland (Seppälä, 2011). By contrast, peat plateaus are usually contiguous and spatially extensive but are also shorter, rarely exceeding 2 metres in height (Dyke & Sladen, 2010).

A great deal of variation in peatland permafrost features exists globally, with characteristics such as shape, active layer depth, and overlying vegetation all varying from region to region. For example, peat plateaus in western Canada tend to be forested (predominantly black spruce [*Picea mariana*]), whereas in Scandinavia, they are covered by lower vegetation, such as lichen, graminoids, and dwarf shrubs (Carpino et al., 2021; Johansson et al., 2013). Such differences in vegetation cover can alter local snow redistribution and summer shading effects, thereby impacting the ground thermal regime (Jean & Payette, 2014a, 2014b).

Climate change has led to rapid peatland permafrost degradation over the past century (Borge et al., 2017; Mamet et al., 2017; Wang et al., in press), with accelerated thaw expected in the coming decades (Fewster et al., 2022). Landform morphology has been previously identified as an important consideration for local surface energy balance and for understanding rates of landform thaw including fragmentation (Mamet et al., 2017; Wang et al., in press).

In Labrador, northeastern Canada, peatland permafrost has been largely understudied until recent years (Brown et al., 1975; Way et al., 2018). Large swaths of land spanning 7° latitude along the Labrador Sea coastline were recently shown to contain hundreds of peatland permafrost complexes, including some of the southernmost features in the Northern Hemisphere (Wang et al., 2023). While prior research has focused on feature identification there is still a need for localised site characterization, especially in the more southern peatlands which are presumed to be at a greater risk of degradation (Hugelius et al., 2020). Understanding the local context of these features is essential in predicting thermokarst potential and habitat change susceptibility.

In this study, we investigate and characterise the contemporary state of 20 peatland permafrost complexes from the southern end to the northern end of the discontinuous permafrost zone in Labrador, as defined by the Permafrost Map of Canada (Heginbottom et al., 1995). We use the contemporary state of southern sites as a substitute for future conditions at northern sites following future climate warming, analogous to a space-for-time substitution (Blois et al., 2013). We additionally evaluate the thermokarst potential and thaw resiliency of peatland permafrost throughout coastal Labrador. This study provides much needed context for an understudied region of Canada, allowing local land managers and rights-holders to better understand and prepare for projected changes in berry-picking habitat, caribou foraging grounds, and carbon stores.

Study Area

Coastal Labrador (51.4°N to 60.3°N) includes over 8,000 km of coastline under the strong synoptic influences of the cold Labrador Current and the position of the Polar Front (Barrette et al., 2020). Mean annual air temperatures range from -12°C near the northern tip to +1.5°C in southern areas near the Strait of Belle Isle (Karger et al., 2017; Karger et al., 2018; Wang et al., 2023; Way et al., 2017). Geologically, Labrador contains mostly igneous and metamorphic bedrock covered by extensive glacial till (Bell et al., 2011; Roberts et al., 2006; Wang et al., 2023). Medium- and fine-grained marine and glaciomarine sediments are common in lowland coastal areas, creating suitable conditions for peatland permafrost development (Hagedorn, 2022; O'Neill et al., 2019; Wang et al., 2023). Coastal ecotypes are primarily characterized by coastal barrens, with dense patches of forest found in select sheltered locations (Roberts et al., 2006; Wang et al., 2023). Wetlands are widespread along the coast, with most wetlands along the southern coastline classified as raised bogs (Foster & Glaser, 1986; Wang et al., 2023).

Materials and Methods

Site selection

A total of 20 peatland permafrost complexes in coastal Labrador were examined using uncrewed aerial vehicles (UAVs) and local field surveys (Table 1; Figure 1; Figures S1-S20). Potential sites were identified using 0.5 m resolution Maxar (Vivid) optical satellite imagery (available as basemap imagery in ArcGIS Online), local knowledge from community members, and a recent inventory of peatland permafrost complexes in coastal Labrador (Wang et al., 2023). Site selection prioritised accessibility, contemporary usage by residents, availability of pre-existing data and monitoring infrastructure, and site representativeness of regional conditions. The peatland complexes examined in this study cover a range of latitudes, mean annual air temperatures, coastal proximities, degradation states, and disturbance levels (Table 1; Figures 1-2) (Way et al., 2017). It should be noted that there is a risk of survivorship bias at southern sites since features near Blanc-Sablon and Red Bay are amongst the last remaining complexes in the area, whereas the central and more northern complexes were sampled across a broader range of site conditions (Wang et al., 2023).

Data collection

Recent advances in uncrewed aerial vehicles (UAV) and photogrammetry techniques like structure-from-motion (de la Barreda-Bautista et al., 2022; Fraser et al., 2020; Westoby et al., 2012) have allowed researchers to create centimeter-precise three-dimensional models of landforms (Van der sluijs et al., 2018). At each of the 20 study sites, UAV surveys with 80% image overlap were collected at heights of 60 or 90 m above the ground surface to balance survey extents with ground sampling distances (Table 1). Surveys followed the Transport Canada guidelines for basic and/or advanced flight operations where applicable. Flights used a DJI Mavic 2 Pro or Autel EVO II Pro quadcopter, flown along double grid flight plans created using the PIX4Dcapture or Autel Explorer flight planning apps, respectively. A minimum of four ground control points (GCPs) were collected at each site to optimize both accuracy and time efficiency (see Assmann et al., 2019); GCP points were collected using an EOS Arrow Gold GNSS or a Bad Eld Flex GNSS with satellite-based Atlas real-time kinematic corrections (4.8 cm to 10 cm vertical root mean square error) (Table 1). Frost probing and instantaneous ground temperature measurements were used to validate permafrost presence or absence in the field at 547 locations, and landform heights were measured at 105 points using an Abney level or clinometer.

Image processing and classification

UAV imagery was processed in PIX4Dmapper 4.7.3 and 4.8.1 at full scale with points requiring a minimum of three image matches between photos (de la Barreda-Bautista et al., 2022; Fraser et al., 2020; Westoby et al., 2012). Orthomosaics and point clouds were generated for each site at a resolution equal to the ground sampling distance (GSD) and then imported into Esri ArcGIS Pro 3.0.3 for derivation of elevation products and digitization of features (Figures S21-S40). Ground points in point clouds were classified using ArcGIS Pro's automated classification tool, set to a standard classification scheme (Figure 3). The tool's performance was visually assessed in vegetated areas and iteratively updated to apply more conservative classification schemes when performance was unsatisfactory in areas of thick vegetation.

DTM and DSM generation

A digital terrain model (DTM) and digital surface model (DSM) were created for each site from the point cloud data exported from PIX4Dmapper. Ground classified points (Figure 3) were converted to a multipoint layer and then interpolated with inverse distance weighting to create a continuous DTM raster with 5 cm resolution. The DSM was generated by sampling for the maximum point cloud return within a 5 cm window similar to Fraser et al (2020). Final DTM and DSM resolutions were chosen to be approximately two times the ground sampling distance of each survey.

Permafrost landform delineation

Palsas and peat plateaus were manually delineated in ArcGIS Pro using each site's RGB orthomosaic and DTM (Figure 4A-4C; Figures S21-S40). Permafrost mounds were distinguished in the orthomosaic by their white-grey lichen cover (e.g., *Cladonia arbuscula, Cladonia rangiferina*, *Ochrolechia frigida*) or visibly exposed peat (Figure 4A-4C; Figure S20-S41), which contrasted with the green, yellow and pink vegetation (e.g. *Sphagnum* spp., *Carex* spp.) of nearby wet depressions. Palsas and peat plateaus were also identified by their elevation, appearing raised and relatively even in the DTMs compared to their surroundings (Figure 4A-4B). Only the largest and most obvious permafrost features could be delineated due to the degraded state of many of the features, making these tracings a conservative estimate of permafrost extent. The presence or absence of frozen ground was also determined in the field using frost probing and/or instantaneous ground temperature profiles (Way & Lewkowicz, 2015) at a total of 547 locations and these data were used to inform feature delineation (Figure 5; Figures S20-S40). The geolocated validation points, feature areas and perimeters were all evaluated and summarized in ArcGIS Pro.

Peatland permafrost landform/patch indices

Each polygon feature traced at a site was considered a single contiguous permafrost landform, or "patch". A series of indices were calculated here to gather information on the shape, size and distribution of patches within a given wetland. Mean patch fractal dimension

(MPFD) provides an average measure of shape complexity at each study site, with larger values indicating more complex shapes. More complex shapes have larger surface areas, which can increase the lateral heat transfer from adjacent unfrozen terrain (Devoie et al., 2021; Mamet et al., 2017). MPFD is calculated as:

$$MPFD = \frac{\sum_{i=1}^{n}\left(\frac{2 \ln p_i}{\ln a_i}\right)}{n} \quad [1]$$

where p is the patch perimeter, a is the patch area, n is the total number of patches, and i is each individual patch (McGarigal & Marks, 1995). MPFD was calculated using FRAGSTATS software (McGarigal & Marks, 1995).

Fragmentation of permafrost features was also assessed using the patch fragmentation index (PFI), calculated as:

$$PFI = \frac{4}{5} \cdot \left(1 - \frac{Ap}{Ai}\right) + \frac{1}{5} \cdot \left(\frac{MPFD}{2}\right) \quad [2]$$

where Ap is total patch area, Ai (area of influence) is the total area that the landform could have covered if it had not undergone fragmentation or degradation, and MPFD is the mean patch fractal dimension (McGarigal & Marks, 1995; Rivas et al., 2022). The total area of the bog captured within the survey was used to approximate Ai (Figures S21-S40), and parts of the bog not captured in the survey were excluded, since permafrost abundance in these areas is unknown. Higher values of PFI represent increased avenues for lateral heat transfer, thereby creating greater thaw susceptibility.

Peatland permafrost landform characteristics

Determining the height of palsas and peat plateaus relative to the surrounding bog presented a unique challenge due to natural undulations and sloping terrain. Comparing the altitude of a palsa to the mean altitude of the unfrozen bog led to substantial under- or over-estimations compared to field-derived height measurements. To address this issue, surface elevations were measured at randomly generated points within the mapped permafrost area (n=1000) and in nearby unfrozen terrain within 5 m of feature outlines (n=1000) (Figure 3D). No points were generated within a 0.5 m buffer on either side of feature outlines to account for mapping uncertainties. Heights were calculated as the difference in elevation between each random point on the permafrost feature and the nearest point in the unfrozen terrain; in the rare case where a polygon did not contain a randomly generated point, heights were manually calculated using the DTM. These sample points (n=1000) were also used to extract vegetation heights overlying permafrost features by differencing the DSM and the DTM at each point location.

Finally, landforms with greater excess ice or a higher ice content require more energy to thaw due to latent heat effects (Hayashi et al., 2007). Above-ground landform volume was used to estimate the amount of excess ice within permafrost features (Lewkowicz et al., 2011). The volume for each individual polygon feature was estimated assuming a hemi-ellipsoidal shape, calculated as:

[3] $$V = 2/3 \cdot \pi \cdot r^3 \text{, or}$$

$$V = 2/3 \cdot basal\ area \cdot maximum\ height$$

Total volume was divided by the site area, providing a standardised estimate of average volumetric excess ice content (VEIC) per m^2.

Relative resiliency index

A novel resiliency index was developed to quantitatively assess relative thaw vulnerability across the 20 study sites. This index incorporated three metrics that could affect the surface energy balance: percent area of bog underlain by permafrost, PFI, and VEIC. Sites with higher permafrost areas and ice contents are assumed to require more overall energy to thaw, resulting in higher resiliency. By contrast, fragmentation increases the surface area directly exposed to lateral energy exchanges, decreasing landform resiliency; PFI values were therefore inverted prior to calculations. Each metric was normalised to range between 0 and 1, then all three indices were averaged for each site. All metrics were equally weighted in the resiliency index because the relative controls on peatland permafrost resiliency have not yet been properly assessed in the region.

Latitudinal trends

Regional means of six different variables (PFI, MPFD, resiliency, percent area, maximum feature height, and VEIC) were also compared to latitude to examine coarse spatial trends in the results (Figure 9).

Results

Permafrost patch characteristics

Total permafrost area mapped per site ranged from 402 ± 8 m^2 at CW5 to 68,957 ± 1,251 m^2 at NA2, with a median value of 8,285 m^2 (Table 2). Percent permafrost coverage, calculated as the total permafrost area divided by the area of the bog captured in the survey multiplied by 100, ranged from 0.59 ± 0.01% at CW5 to 58.73 ± 0.90% at CW1, with a median value of 10.2% (Table 2). The sites with the largest permafrost extents were found near Nain, Rigolet and Cartwright, however sites with small extents are found in all regions. Apart from CW1 and NA2, all sites had less than 30% permafrost coverage.

The total number of permafrost patches per site ranged from 2 at CW1 to 88 at RB4, with a median number of patches of 17 (Table 2). Average patch area ranged from 42 m^2 at CW4 to 14,233 m^2 at CW1 (Table 2). Notably, the Sandwich Bay region adjacent to the community of Cartwright included both the site with the smallest average patches and the site with the largest average patches. Median patch size across all sites was 259 m^2.

Maximum vegetation height ranged from 0.02 ± 0.01 m at CW2 to 1.58 ± 0.11 m at RG3, with a median value of 13 cm across all sites (Table 2). Tall or shrubby vegetation (i.e., vegetation height > 50 cm) was found at two sites near Cartwright, two sites near Rigolet, and one site near Nain, but was not found at any sites near Black Tickle, Blanc-Sablon, or Red Bay (Table 2). Notably, maximum vegetation height was below the detectable limit at BT2 (0.04 ± 0.12 m), RB1 (0.07 ± 0.09 m) and RB2 (0.08 ± 0.14 m) (Table 2). Average vegetation height was less than 3 cm at each site, with a study-wide mean vegetation height of approximately 1 cm.

Shape and fragmentation indices

MPFD provides information on two-dimensional landform shape complexity, with values closer to 1 indicating simple geometries such as squares or circles whereas values closer to 2 indicate complex shapes with complicated perimeters (McGarigal & Marks, 1995). MPFD values at the sites ranged from 1.03 at RB4 to 1.30 at CW4, with a median MPFD value across all sites of 1.22 (Table 3). These low values indicate that peatland permafrost landforms in Labrador have relatively simple shapes and perimeters.

PFI, an index of landform fragmentation, was used to assess permafrost patch fragmentation at each study site. Fifteen out of the twenty study sites had a PFI over 0.8, which is considered a very high level of fragmentation (Rivas et al., 2022). Four sites had PFIs between 0.6 and 0.79, considered to be highly fragmented, and one site (CW1) had a PFI index value in the medium fragmentation category (0.4 to 0.59).

Feature heights and volumetric excess ice contents

Site-level mean feature heights were calculated using the maximum height from each permafrost patch. Mean feature heights ranged from 0.15 m at RB1 to 1.8 m at NA1, with a median value of 0.5 m across all sites (Table 2). Similarly, maximum feature heights ranged from 0.21 ± 0.09 m at RB1 to 3.7 ± 0.12 m at NA1, with significant within and across site variability (Figure 6; Table 2).

The estimated median volumetric excess ice content (VEIC) across all sites was 0.034 m^3 of excess ice per m^2. VEICs ranged from 0.001 m^3/m^2 (RB1) to 0.263 m^3/m^2 (CW1), with the highest regional variability found near Rigolet and Cartwright (Figure 7). Notably, all sites near Red Bay and Blanc-Sablon reported VEICs below the study wide median VEIC.

Vulnerability assessment

Eleven out of the twenty sites were classified as having very low thaw resiliency (0 - 0.2) while seven had low thaw resiliency (0.2 - 0.4) (Figure 8, Table 3). Only two sites were considered to have high (0.6 - 0.8) or very high (0.8 - 1) resiliency, with one site near Cartwright (CW1) and another near Nain (NA2) (Figure 8, Table 3).

Spatial trends

Statistically significant ($p<0.05$) positive latitudinal relationships were observed for resiliency, maximum feature height, and VEIC (Figure 9). MPFD also showed a statistically significant non-linear (2^{nd} order polynomial) association with latitude, wherein MPFD values were low at the southernmost and northernmost sites but high at sites in central Labrador.

Discussion

Characterisation of peatland permafrost in Labrador

Investigated peatland permafrost complexes in coastal Labrador varied in size, characteristics, morphology, and fragmentation. Average landform size ranged from 42 m^2 at a southern site to 14,233 m^2 at a central outer-coast site (Table 2). Sites near the southern end of the study area often contained only a few isolated patches of permafrost, while others farther north near Black Tickle, Cartwright, and Rigolet included more intact peat plateaus. Landform sizes reported in this analysis fall within the ranges reported by other studies (Allard & Rousseau, 2002; Dyke & Sladen, 2010; Emmert & Kniesel, 2021; Fillion et al., 2014; Pironkova, 2017, Verdonen et al., 2022). For example, Pironkova (2017) reported features ranging from 10 m^2 to 117,894 m^2 in northern Ontario, with 75% of all mapped features ranging between 50 m^2 and 3,000 m^2 (Pironkova, 2017). Landforms in Québec, northwestern Canada, Iceland, and Scandinavia were reported to range in size from 30 m^2 to 4,000 m^2, with landform areas appearing comparable between all four regions (Allard & Rousseau, 2002; Dyke & Sladen, 2010; Emmert & Kniesel, 2021; Fillion et al., 2014; Pironkova, 2017, Verdonen et al., 2022). The smallest observed permafrost patches from this study often skewed smaller than those described in other regions; however, this is likely due to our use of UAVs which generated higher resolution imagery than many of the satellite-imagery based studies.

Generally, landform heights in coastal Labrador are more comparable to observations from northern Ontario and Scandinavia than features described in northern Québec, the Northwest Territories, and Yukon Territory (Allard & Rousseau, 2002; Dyke & Sladen, 2010; Emmert & Kniesel, 2021; Fillion et al., 2014; Pironkova, 2017, Verdonen et al., 2022). Most palsas and peat plateaus in this study were less than 1 metre tall, with the tallest features within a given complex rarely exceeding 2 metres (Table 2; Figure 6). Landforms near Attawapiskat, Ontario (52.9°N) are described as 1 m tall or less (Pironkova, 2017), which is similar to the maximum feature heights found near Blanc-Sablon (51.5°N) and Red Bay (51.8°N) presented in our analysis (Table 2; Figure 6). However, permafrost landforms between 55.1°N and 57.6°N in northern Québec were reported to range from 2 m to 6 m (Allard & Rousseau, 2002; Fillion et al., 2014), whereas maximum feature heights near Nain (56.6°N) only reached 3.65 ± 0.12 m (Table 2).

Like previous studies, we observed a correlation between maximum landform height and latitude (Figure 9) with northern sites containing taller features than most southern sites (Allard & Rousseau, 2002; Pironkova 2017). However, considerable variability in feature heights within and across sites suggests that other factors, such as surficial deposits, human and wildlife disturbance, and local microclimate (e.g., coastal proximity), also play an important role in promoting taller landforms (Figure 6). Sites on outer islands and/or directly on the coast (e.g., CW1, RB4) were typically larger and less fragmented than inland sites (e.g., CW4, RB1) in the same area, indicating that coastal microclimate could be a key factor for landform resilience in Labrador (Table 2; Table 3). Sites with evidence of heavy human disturbance such as skidoo trails (e.g., CW4), also exhibited higher levels of fragmentation than other less disturbed complexes in the same region (Table 3).

Most peatland permafrost complexes were dominated by lichen cover (e.g., *Ochrolechia frigida, Cladonia rangiferina*), dwarf shrubs (*Betula glandulosa, Empetrum nigrum, Vaccinium uliginosum*), and short herbaceous vegetation (*Rubus chamaemorus*), with average vegetation heights below 3 cm at all sites. While five sites contained vegetation taller than 50 cm (Table 2), only one of these sites (NA1) exhibited tall vegetation cover in more than a single isolated patch. This is in stark contrast to other parts of Canada, where peatland permafrost is densely forested (*Picea mariana*) (Baltzer et al., 2014; Carpino et al., 2021; Pironkova et al., 2017). While palsas in Québec reported similarly short vegetation near their tallest points, they also tend to support tall trees along edges (Allard & Rousseau, 2002). As such, we consider the complexes described in coastal Labrador to be more similar to those described in Iceland and Scandinavia, which are characterised by lichen, moss, and dwarf shrub vegetation cover (Emmert & Kniesel, 2021; Verdonen et al., 2022).

Resilience of peatland permafrost complexes and ecosystems

The space-for-time substitution transect presented in this study provides important insights into the future evolution of peatland permafrost in coastal Labrador. In particular, the complexes found near Blanc-Sablon and Red Bay are inferred to have low ice contents, low heights, and low resiliency compared to central and northern sites (Figure 9). The results are interpreted to be a result of ongoing climatic warming and subsequent permafrost thaw in the region (Barrette et al., 2020; Wang et al., in press), and likely represent the trajectory of landforms in coming decades.

The estimated volumetric ice contents reported in this study provide an indication of thaw resiliency because of the greater energy required to thaw excess ground ice; however, higher VEIC estimates also indicate greater thermokarst potential. While VEIC was shown to increase with latitude (Figure 9), sites with very low VEIC values were found across a range of latitudes (Figure 7). Sites with the lowest VEIC values were either further inland (e.g., RB1) or contained evidence of human disturbance (e.g., RG2), highlighting the importance of local-scale factors in maintaining landforms.

Four of the sites in this study have been previously visited by other researchers, who documented heights and general characteristics of the landforms at the time. Palsas and peat plateaus at CW5 were reported to be 1.5 m tall when visited in 1968 (Brown, 1975) and 1.0 m tall in 2014 (Way et al., 2018). The tallest reported height from our 2021 field visit was 0.7 m, indicating an accelerated rate of thaw in recent years (Table 2). Similarly, between 2014 and 2021, reported maximum heights decreased from 1.0 m to 0.8 m at RB2, 1.4 m to 1.1 m at BS1, and 1.3 m to 0.6 m at CW4 (Table 2) (Way et al., 2018). Visual evidence of feature degradation, including thermokarst ponding, exposed peat, and peat cracking, were present at every site within this study, indicating ongoing thaw-related ecosystem and landscape modification. These results align with recent analyses by Wang et al. (in press), who reported substantial thaw of peatland permafrost landforms at seven locations in coastal Labrador since as early as 1948.

The vast majority (95%) of study sites exhibited high or very high levels of fragmentation, with no significant latitudinal relationship (Table 3; Figure 9). However, a 2nd order polynomial fit between latitude and MPFD suggested peak MPFD occurred in the central portion of the study transect (Figure 9). Mamet et al. (2017) noted this type of pattern may reflect an increase in landform shape complexity during initial thaw stages, followed by a decrease in complexity in later degradational stages. This pattern could also be indicative of the presence of taliks or expanded vegetation patches accelerating thaw along uneven boundaries, creating irregular landform shapes (Devoie et al., 2021; Jean & Payette, 2014b). Theoretically, continued thaw would lead to accelerated thaw on lateral margins and protrusions formed during initial fragmentation stages, resulting in a return to simpler landform shapes (Mamet et al., 2017).

Our index-based assessment of relative peatland permafrost resiliency suggests that most of our study sites are highly vulnerable to thaw (Figure 8). All sites south of 53.8°N (n=13) were considered to have low or very low resiliency relative to other complexes in the region (Figure 8). Mean annual air temperatures of +1.5°C at southern sites are already near previously established thresholds for the maintenance of permafrost (Shur & Jorgenson, 2007; Way et al., 2017); therefore, recent climatic warming (Barrette et al., 2020) has likely negatively impacted these complexes. Sites with peat plateaus generally had higher relative resiliency indices than comparably situated palsa sites (Table 3; Figure 8). Recent work from elsewhere in coastal Labrador has observed slower thaw rates for peat plateaus compared to palsas, suggesting a link between landform morphology and resiliency (Wang et al., in press).

Only two sites in this study (NA2 and CW1) were classified as having a high or very high thaw resiliency. These two sites contained more permafrost, taller features, and relatively minimal evidence of ongoing fragmentation processes compared to other sites in the region. However, even these high resiliency sites contained evidence of thaw such as peat cracking and thermokarst ponding (Sollid & Sorbel, 1998; Luoto & Seppala, 2003). The relative resiliency index may therefore overestimate resiliency levels, though it would be difficult to rectify this without finding a model study site for comparison.

Impacts of thaw

The dry, lichen-dominated vegetation found on unforested peatland permafrost tends to shift towards wet-sedges, mosses, and tall shrubs following feature degradation (Bosiö et al., 2012; Christensen et al., 2004). These shifts are expected to have significant negative consequences for cultural keystone wildlife species for Labrador Inuit and Labrador Innu, such as caribou (Borish et al., 2021; Schmelzer et al., 2020). It is estimated that peatlands cover 40% of the habitat used by the threatened Mealy Mountain caribou herd, with elevated lichen-rich permafrost mounds potentially comprising important winter forage for the herd (Errington et al., 2022; Kumpala 2004; Schmelzer et al., 2020). Six of our study sites overlap with the Mealy Mountain herds range, with four of these sites demonstrating very low resiliency and one exhibiting low resiliency (Figure 8). Peatland permafrost degradation increases local snow depths, increases summer wetness, and alters plant community composition, which could in-turn decrease winter forage quality in the region (Anderson et al., 2018; Istomin & Habeck, 2016; Johnson, 2022; Markkula et al., 2019). However, some studies suggest that thaw could result in increased total forage biomass, so the net effect of these projected changes for local herds remains uncertain (Istomin & Habeck, 2016; Markkula et al., 2019).

Previous research has also shown palsa and peat plateau subsidence often results in a shift from dry, uplifted features towards flat, water-saturated terrain (Disher et al., 2021) with direct impacts on local plant communities (Arlen-Pouliot & Bhiry, 2005). Bakeapples (appik, shikuteu, cloudberries, *Rubus chamaemorus*) are a culturally important berry species that are typically abundant on palsas and peat plateaus (Anderson et al., 2018). While initial landform thaw may increase nutrient availability for these plants, bakeapples are not well-adapted to long term survival in wet environments (Keuper et al., 2017; Markulla et al., 2019). Results from this analysis suggest likely widespread degradation of peatland permafrost in the near-future (Figure 8), which would reduce the abundance and accessibility of important berry-picking grounds (Markkula et al., 2019).

Limitations

Using UAVs in this study allowed us to efficiently compare indices across highly variable sites. However, only a handful of previous studies have used UAVs for similar purposes (de la Barreda-Bautista, 2022; Verdonen et al., 2022), thus it was difficult to assess our results in comparison to other regions. Additionally, among peatland permafrost studies that describe geomorphological parameters, there are inconsistencies in how these data are reported. For example, permafrost area was variably reported as the total area at a site, the total area for a large region, by average landform size, or by individual landform area/diameters, depending on the study (Allard & Rousseau, 2002; Borge et al., 2017; Dyke & Sladen, 2010; Emmert & Kniesel, 2017; Mamet et al., 2017; Pironkova, 2017; Verdonen et al., 2022). Furthermore, characteristics such as height, volume, and fragmentation are sparse within the literature. Providing more comprehensive and descriptive geomorphological parameters in peatland permafrost studies would enhance the ability for researchers to compare site characteristics.

Many of the wetlands in coastal Labrador cover several km^2 with unclear boundaries, making it difficult to collect UAV imagery for the entire bog. Survey areas tried to prioritise areas with high landform density, however it is important to note that the reported values should only be discussed in relation to the survey area, not to the overall wetland. As UAV technology improves and battery life extends, larger surveys could be paired with high resolution satellite imagery to help improve these statistics. Site access was also a major challenge, so some regions with high densities of peatland permafrost were not surveyed. Further work in the regions between Rigolet and Nain would improve our understanding of the characteristics and potential resiliency of features along this section of the Labrador Sea coastline.

Finally, it is important to consider the potential for survivorship bias when assessing the contemporary characteristics of peatland permafrost complexes in southern Labrador. This study examined sites where permafrost currently persists, and thus did not examine fully thawed sites that previously contained permafrost. The limited number of peatland permafrost complexes still present in southern Labrador may be representative of the most resilient landforms of a formerly larger population of peatland permafrost complexes. Therefore, while these southern sites can be used to extrapolate out the future state of some northern features, it is important to remember that other peatland permafrost complexes may degrade altogether.

Conclusion

High-resolution UAV surveys of peatland permafrost spanning from 51.4° N to 56.5°N along the Labrador Sea coastline provide insight into the characteristics and vulnerability of peatland permafrost complexes in the region. Permafrost landform height, extent, and vegetation cover at surveyed sites in Labrador were more similar to features described in northern Europe than the larger, more heavily vegetated features found in western Canada. A novel relative resiliency index derived in this study indicates that most peatland permafrost complexes in the region have a low thaw resiliency, making them vulnerable to degradation in the near future. This is the first large-scale descriptive study of peatland permafrost within Labrador and provides the baseline geomorphological information necessary for future modelling, change assessment, and land management projects in this understudied region of Canada.

Acknowledgements

The authors of this paper would like to acknowledge our many funders, collaborators, and community partners, without whom this work would not have been possible. Thank you to the Natural Sciences and Engineering Research Council of Canada, the Northern Scientific Training Program, the Canadian Foundation for Innovation, Queen's University, the Ontario Research Fund and the Ontario Graduate Scholarship program for their funding contributions for travel, equipment, and stipend costs related to this project. We are grateful to the Nunatsiavut Government (Rodd Laing), the Nunatsiavut Research Center (Frédéric Dwyer-Samuel, Caroline Nochasak, Michelle Saunders, Carla Pamak, Liz Pijogge), Innu Nation (Jack Feldgajer, Jack Penashue, and Max Penashue) and the NunatuKavut Community Council (Charlene Kippenhuck, George Russell Jr., and Bryn Wood) for their guidance and permission to conduct this research on their traditional territories. Thank you to Patrick Lauriault, Tara Ryan, and Michaela Smitas-Kraas for their assistance with data collection. Thanks to Martin Andersen, Eldred Andersen, Gary Bird, Patrick Davis, Anthony Elson, Jeffrey Keefe, Jeremy Ivany, Reginald Maggo, Tyler Palliser, Derrick Pottle and Martin Shiwak for their boat driving and bear guarding services. Our team is also grateful for the accommodations provided by Tanya Barney, Freeman Butt, Jeffrey Keefe, Wendy Keefe, Barbara Mesher, Karl Michelin, Sandi Michelin, Paulette Pilgrim, Martin Shiwak, and the Nunatsiavut Research Center and for additional in-kind support provided by Caitlin Lapalme, Jack Shiwak, Jane Shiwak, and George Way.

Tables

Table 1. Summary of UAV survey information for peatland permafrost study sites.

Site name	Lat, Long	Date of survey	UAV model	Flight altitude	Study area size (m^2)	GSD (cm/ pixel)	Number of GCPs	Mean GCP VRMS (m)	Site type
NA1	56.49, -61.40	2022-08-26	DJI Mavic 2 Pro	90	99, 256	2.14	6	0.063	Palsa
NA2	56.46, -61.51	2022-08-25	DJI Mavic 2 Pro	90	228, 047	2.14	7	0.052	Palsa
RG1	54.28, -58.27	2021-08-12	DJI Mavic 2 Pro	90	241, 111	2.14	7	0.058	Mixed
RG2	54.16, -58.46	2021-08-09	DJI Mavic 2 Pro	90	249, 925	2.14	8	0.049	Palsa
RG3	54.11, -57.88	2022-08-11	Autel Evo II Pro	90	141, 637	2.04	7	0.054	Mixed
RG4	54.01, -58.56	2022-08-09	DJI Mavic 2 Pro	60	71, 878	1.43	6	0.066	Mixed
CW1	53.85, -56.96	2022-08-14	Autel Evo II Pro	90	131, 577	2.04	6	0.065	Plateau
CW2	53.75, -56.74	2021-08-31	DJI Mavic 2 Pro	90	125, 621	2.14	6	0.062	Plateau
CW3	53.72, -57.10	2021-09-03	DJI Mavic 2 Pro	90	153, 151	2.14	8	0.051	Mixed
CW4	53.71, -57.01	2021-09-02	DJI Mavic 2 Pro	90	172, 102	2.14	8	0.057	Palsa
CW5	53.69, -57.02	2021-08-30	DJI Mavic 2 Pro	90	140, 524	2.14	8	0.060	Palsa
BT1	53.46, -55.81	2022-08-18	DJI Mavic 2 Pro	60	46, 030	1.43	4	0.065	Plateau
BT2	53.46, -55.82	2021-08-29	DJI Mavic 2 Pro	60	67, 777	1.43	7	0.076	Plateau
BT3	53.42, -55.85	2022-08-17	Autel Evo II Pro	60	89, 838	1.36	4	0.054	Mixed
BT4	53.41, -55.83	2022-08-17	DJI Mavic 2 Pro	90	116, 366	2.14	4	0.052	Mixed
RB1	51.81, -56.38	2022-08-01	DJI Mavic 2 Pro	60	54, 313	1.43	5	0.070	Palsa
RB2	51.76, -56.41	2021-07-24	DJI Mavic 2 Pro	60	63,170	1.43	6	0.080	Palsa
RB3	51.75, -56.43	2021-07-26	DJI Mavic 2 Pro	60	63,330	1.43	6	0.088	Palsa
RB4	51.74, -56.41	2021-07-26	DJI Mavic 2 Pro	60	83,050	1.43	6	0.056	Palsa
BS1	51.46, -57.19	2021-08-02	DJI Mavic 2 Pro	60	68, 100	1.43	6	0.070	Palsa

Table 2. Summary statistics on permafrost area, extent, patch number, patch size, feature height and vegetation height for all 20 sites surveyed in this study.

Site	Percent area coverage (%)	Total permafrost extent (m^2)	Number of patches	Average patch size (m^2)	Average feature height (m)	Maximum feature height (m)	Maximum vegetation height (m)
NA1	13.58±0.35	12,151±236	18	655	1.81	3.65±0.12	1.13±0.12
NA2	31.27±0.88	68,957±1,251	34	1,840	0.95	2.18±0.04	0.23±0.04
RG1	14.69±0.70	29,111±582	39	746	0.97	2.63±0.01	0.49±0.01
RG2	3.43±0.04	5,315±106	28	190	0.43	1.00±0.01	0.21±0.01
RG3	9.25±0.28	10,238±205	14	731	0.61	1.37±0.11	1.58±0.11
RG4	9.12±0.43	9,866±197	7	1,409	0.99	1.78±0.09	1.01±0.09
CW1	58.73±0.90	28,402±569	2	14,233	1.16	1.83±0.01	0.12±0.01
CW2	25.75±0.25	19,497±3130	16	1,219	0.63	1.14±0.01	0.02±0.01
CW3	7.90±0.10	6,519±390	36	181	0.52	1.03±0.05	0.52±0.05
CW4	1.41±0.05	2,335±47	56	42	0.20	0.59±0.06	0.57±0.06
CW5	0.59±0.01	402±8	3	134	0.39	0.71±0.08	0.08±0.08
BT1	11.97±0.07	4,623±92	3	1,541	0.80	1.09±0.01	0.04±0.01
BT2	27.24±0.09	7,971±159	28	285	0.39	0.86±0.12	0.04±0.12
BT3	13.69±0.15	10,586±212	10	1,059	0.57	0.94±0.01	0.21±0.01
BT4	9.12±0.25	8,599±172	37	232	0.42	1.10±0.01	0.04±0.01
RB1	2.25±0.90	478±10	8	60	0.15	0.21±0.09	0.07±0.09
RB2	3.58±0.01	1,166±23	22	53	0.39	0.82±0.14	0.08±0.14
RB3	4.10±0.04	990±20	5	198	0.45	0.92±0.09	0.12±0.09
RB4	11.15±0.17	7,857±157	88	89	0.28	0.64±0.01	0.09±0.01
BS1	14.81±0.02	12,151±47	14	169	0.44	1.24±0.08	0.13±0.08

Table 3. Mean patch fractal dimension (MPFD), patch fragmentation index (PFI) and relative resiliency index (RRI) for each study site.

Site	MPFD	PFI	Resiliency
NA1	1.17	0.81	0.38
NA2	1.13	0.66	0.68
RG1	1.18	0.80	0.36
RG2	1.25	0.90	0.04
RG3	1.18	0.84	0.15
RG4	1.19	0.81	0.31
CW1	1.25	0.46	1.00
CW2	1.22	0.72	0.39
CW3	1.22	0.86	0.11
CW4	1.30	0.92	0.01
CW5	1.16	0.91	0.01
BT1	1.28	0.83	0.21
BT2	1.27	0.71	0.37
BT3	1.22	0.81	0.23
BT4	1.20	0.85	0.14
RB1	1.26	0.91	0.02
RB2	1.27	0.90	0.04
RB3	1.25	0.89	0.05
RB4	1.03	0.81	0.17
BS1	1.17	0.80	0.19

Figures

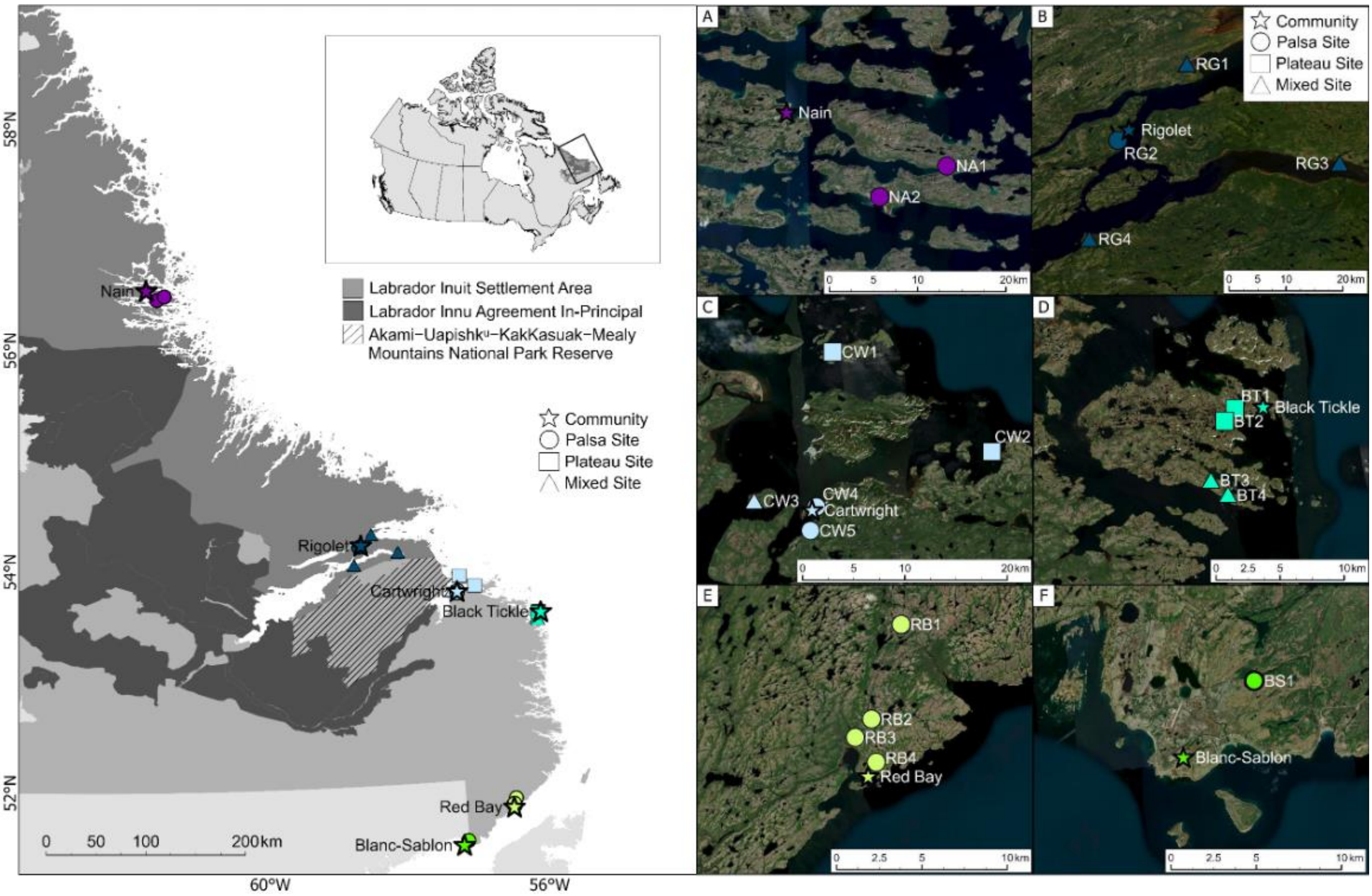

Figure 1. *Left*: Distribution of study sites across coastal Labrador, with inset map showing location of study region within Canada. *Right*: Large scale maps of study sites near the communities of (A) Nain, (B) Rigolet, (C) Cartwright, (D) Black Tickle, (E) Red Bay and (F) Blanc-Sablon. Satellite imagery is sourced from Maxar (Vivid) optical satellite imagery, acquired via the Esri ArcGIS Online World Imagery basemap.

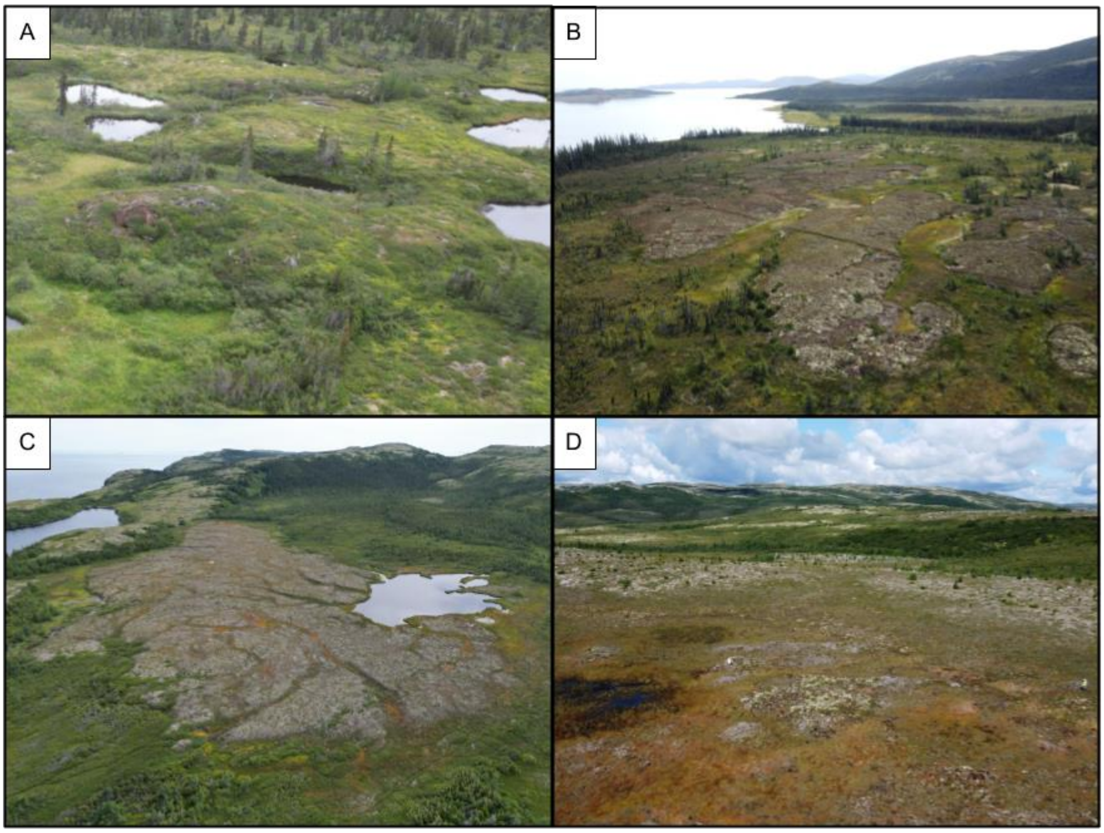

Figure 2. Aerial imagery of (A) NA1, (B) RG1, (C) CW1, and (D) RB1 acquired with a DJI Mini 2 Pro or DJI Mini 3 Pro. The peatland permafrost complexes pictured here demonstrate a variety of sizes, shapes, and degradation states observed in the region.

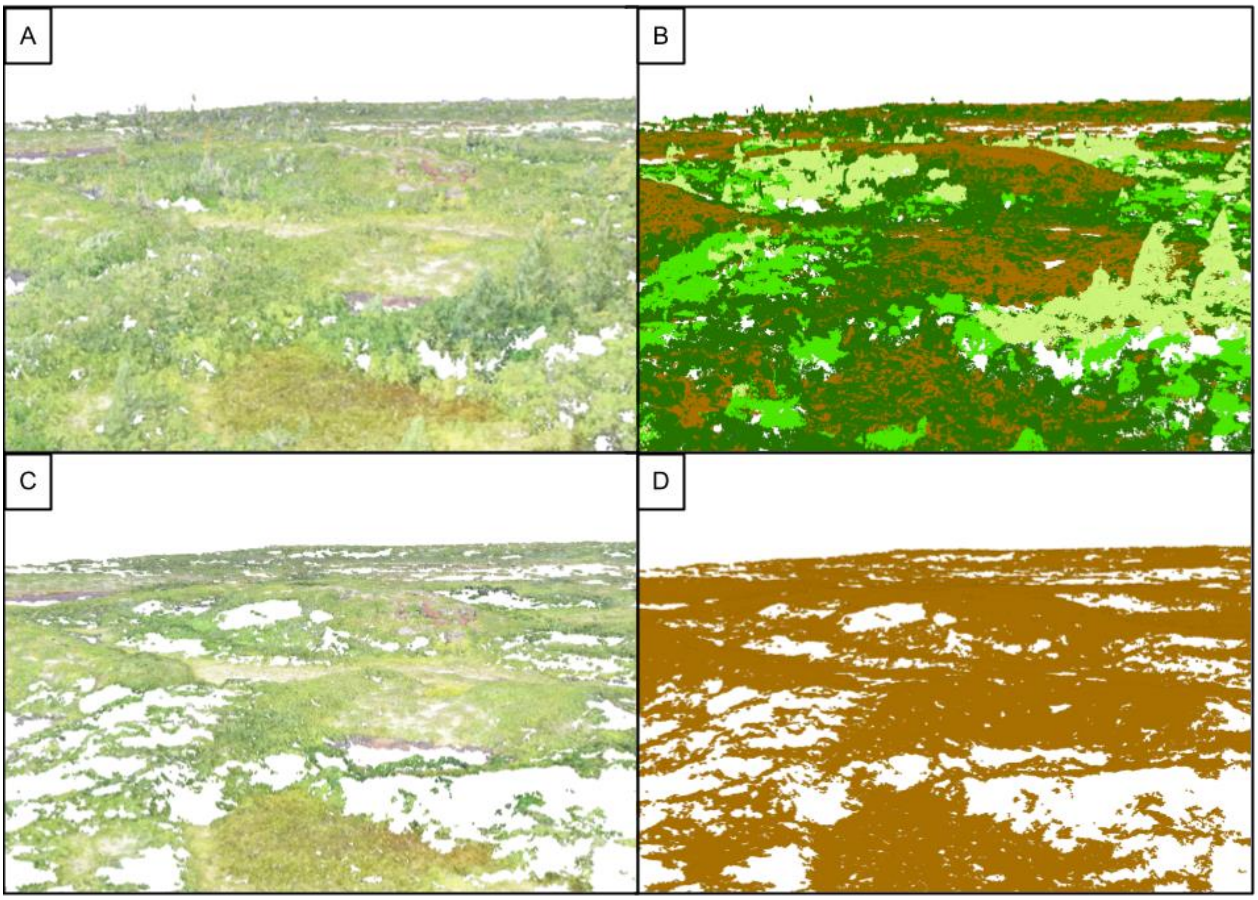

Figure 3: Oblique view of NA1 point cloud showing (A) all points in RGB; (B) all points shown by land cover classification (brown = ground, light green = tall vegetation, medium green= medium vegetation, dark green = short vegetation); (C) ground classified points shown in RGB; and (D) ground classified points shown by land cover classification.

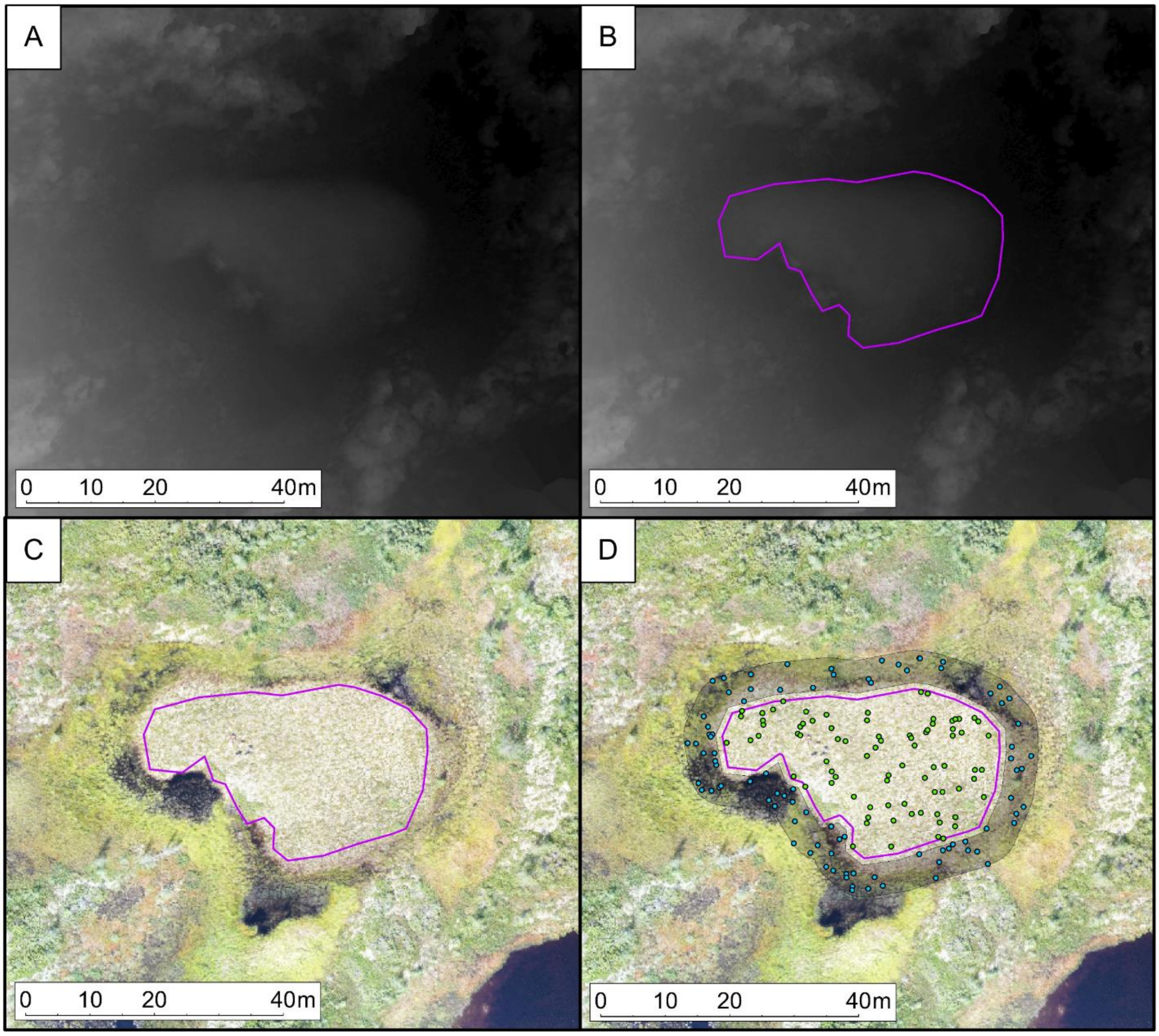

Figure 4. Example of feature delineation and data extraction of a palsa at RG4. (A) DTM, (B) feature tracings overlain on DTM (C) feature tracings overlain on orthomosaic, and (D) feature tracing and corresponding buffer zone of 0.5 m, displaying the location of the randomly generated points on the palsa (green dots) and off the palsa (blue dots).

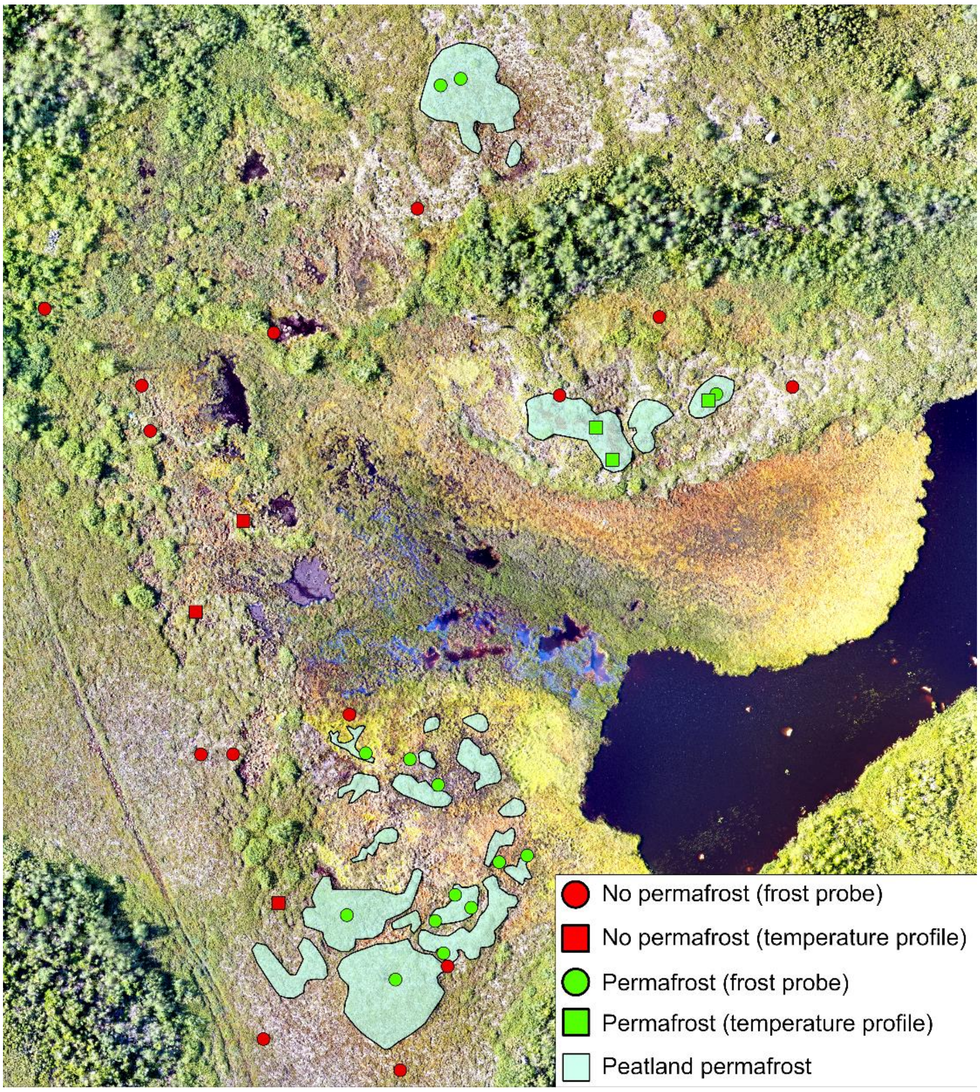

Figure 5: Interpreted peatland permafrost landform extents (green polygons) overlain on a UAV-derived orthomosaic of RB2. Points show probing locations classified according to whether frozen soil was detected (green points = frozen, red points = unfrozen). All probe point locations were collected with a GARMIN GPSMAP 66SR handheld unit (± 1.8 m).

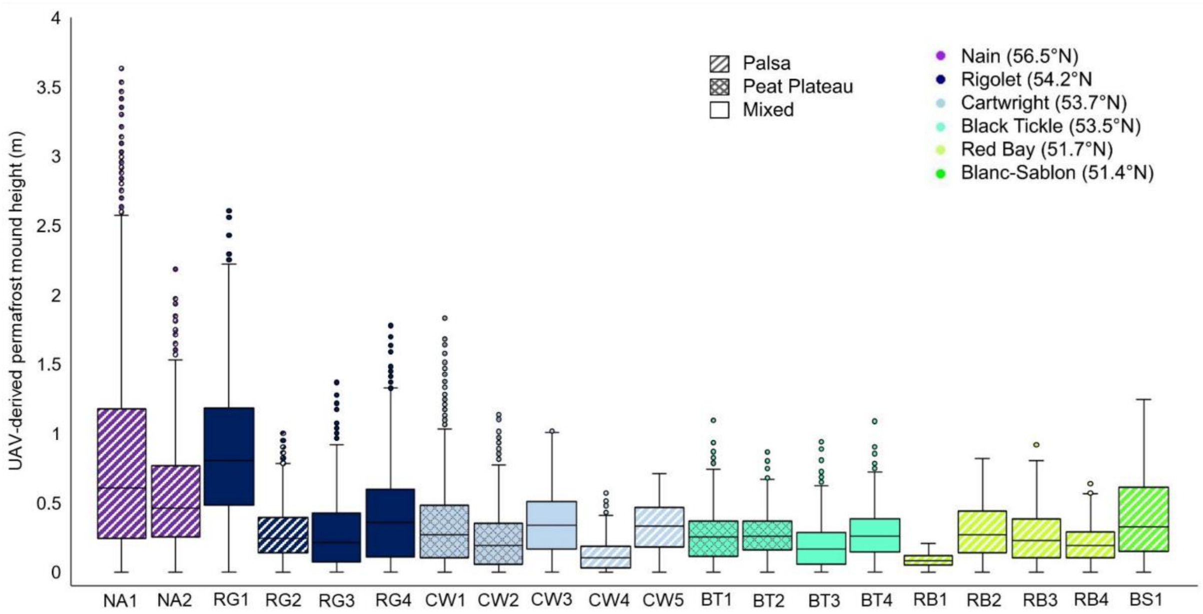

Figure 6. Heights of permafrost mounds from the 1000 randomly distributed matched pairs of peatland permafrost and bog points. Boxes range from 25th percentile to 75th percentile, with the thick black line representing the sample median. Whiskers extend to the minimum and maximum values within 1.5 times the interquartile range. Values outside this range are represented as points.

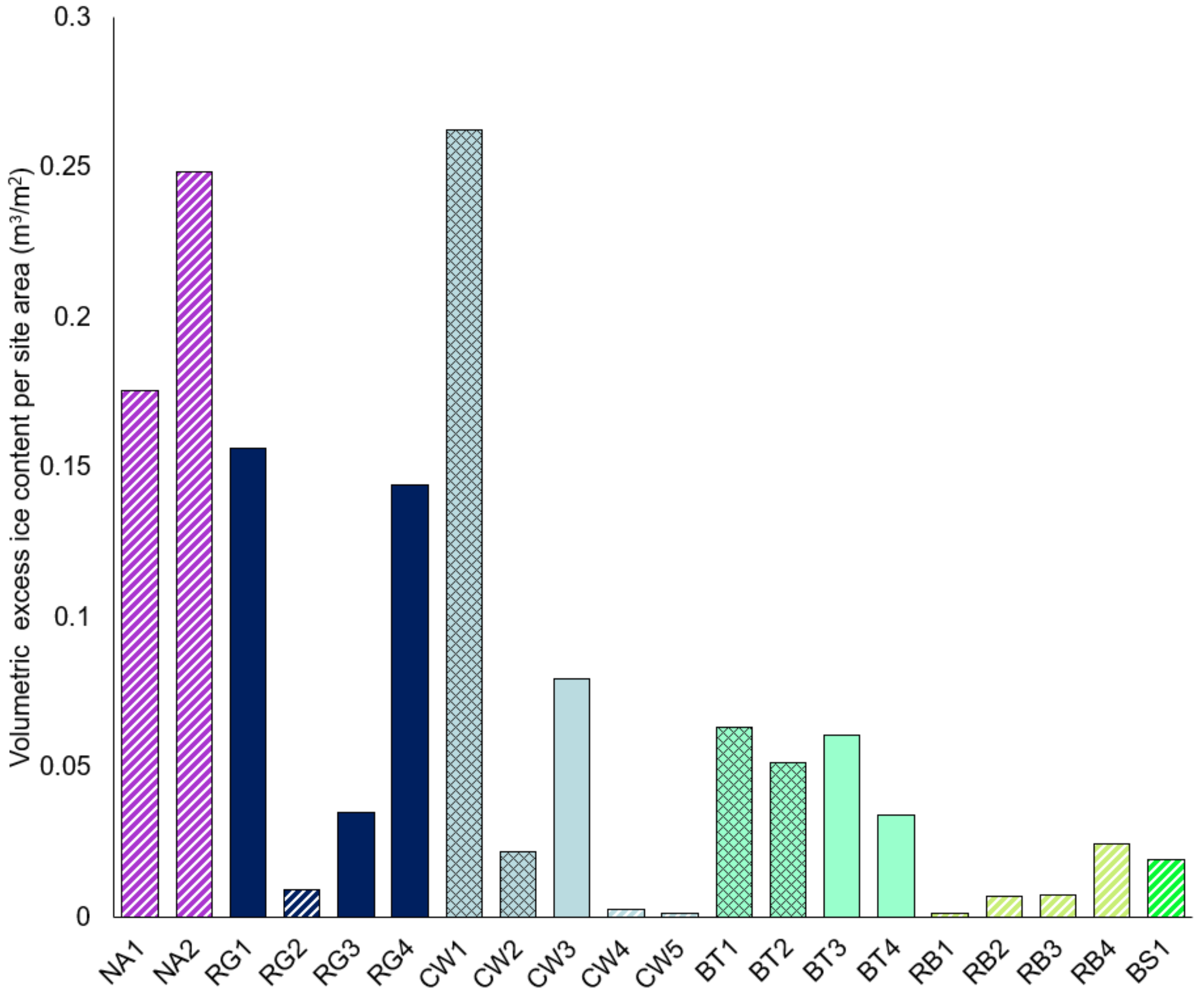

Figure 7. Estimated volumetric excess ice content (m^3) standardised by site area (m^2) for each study site.

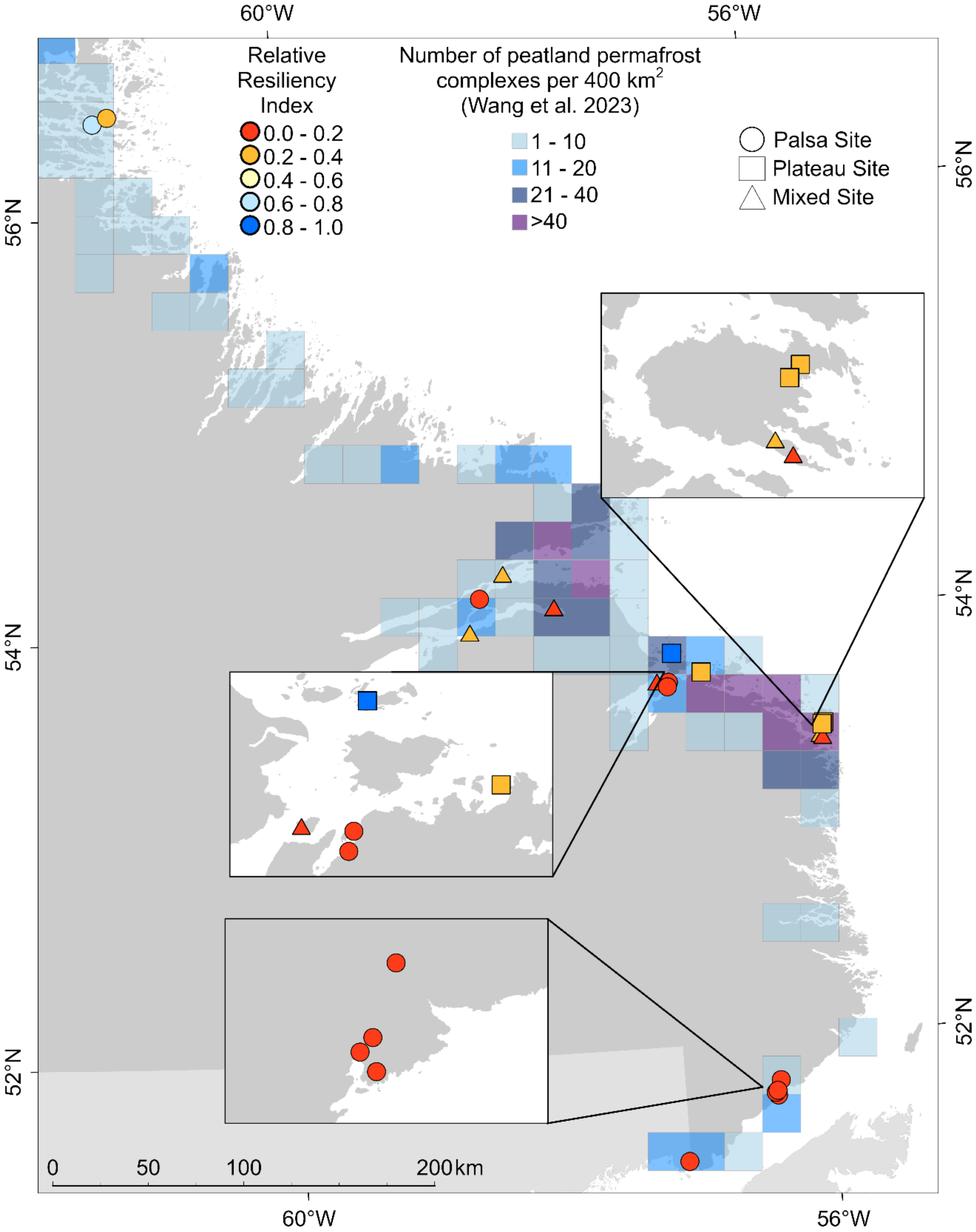

633

634 Figure 8. Thaw resiliency of study sites overlain on a peatland permafrost complex density map

635 in Labrador (Wang et al., 2023).

636

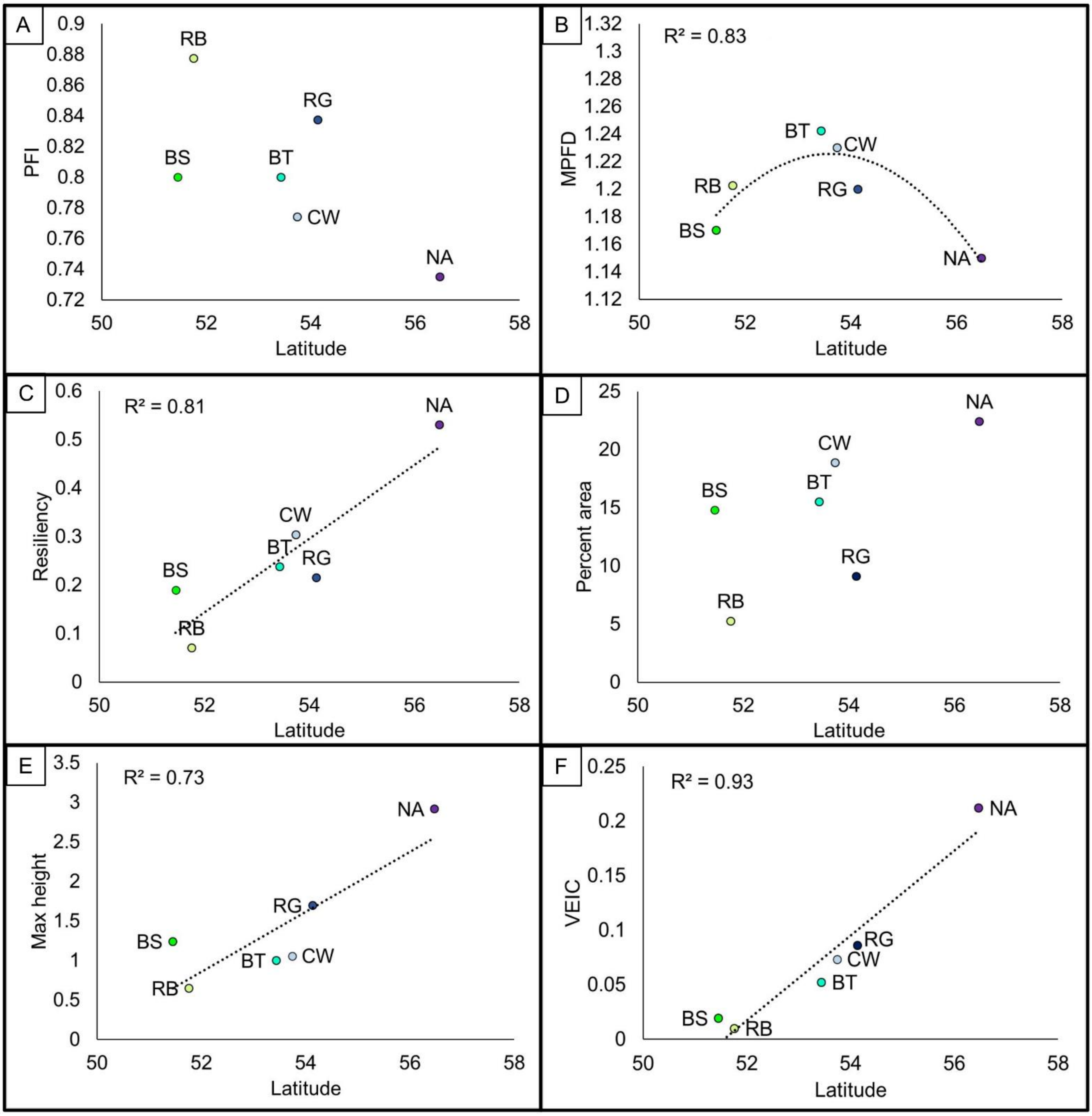

Figure 9. Scatterplots showing the relationships between latitude and (A) PFI, (B) MPFD, (C) resiliency, (D) percent area, (E) maximum height, and (F) VEIC. Points represent the mean value across all study sites near a given community (BS = Blanc-Sablon, RB = Red Bay, BT = Black Tickle, CW = Cartwright, RG = Rigolet, NA = Nain). Significant ($p<0.05$) linear and 2nd order polynomial relationships are shown by trendlines, with corresponding R^2 values shown on plot.

References

Allard, M., & Rousseau, L. (2002). The internal structure of a palsa and a peat plateau in the Rivière Boniface region, Québec: Interferences on the formation of ice segregation mounds. *Géographie Physique et Quaternaire*, *53*(3), 373–387. https://doi.org/10.7202/004760ar

Anderson, D., Ford, J. D., & Way, R. G. (2018). The Impacts of Climate and Social Changes on Cloudberry (Bakeapple) Picking: A Case Study from Southeastern Labrador. *Human Ecology*, *46*(6), 849–863. https://doi.org/10.1007/s10745-018-0038-3

Arlen-Pouliot, Y., & Bhiry, N. (2005). Palaeoecology of a palsa and a filled thermokarst pond in a permafrost peatland, subarctic Québec, Canada. Holocene, 15(3), 408–419. https://doi.org/10.1191/0959683605hl818rp

Assmann, J. J., Kerby, J. T., Cunliffe, A. M., & Myers-Smith, I. H. (2019). Vegetation monitoring using multispectral sensors—Best practices and lessons learned from high latitudes. Journal of Unmanned Vehicle Systems, 7(1), 54–75. https://doi.org/10.1139/juvs-2018-0018

Baltzer, J. L., Veness, T., Chasmer, L. E., Sniderhan, A. E., & Quinton, W. L. (2014). Forests on thawing permafrost: Fragmentation, edge effects, and net forest loss. *Global Change Biology*, *20*(3), 824–834. https://doi.org/10.1111/gcb.12349

Barrette, C., Brown, R., Way, R.G., Mailhot, A., Diaconescu, E.P., Grenier, P., Chaumont, D., Dumont, D., Sévigny, C., Howell, S., and Senneville, S. (2020). Nunavik and Nunatsiavut regional climate information update, second iteration. In Nunavik and Nunatsiavut: From science to policy. An Integrated Regional Impact Study (IRIS) of climate change and modernization. Edited by P. Ropars, M. Lemay, and M. Allard. ArcticNet, Québec City, Canada. pp. 1–66.

Bell, T., Putt, M., and Sheldon, T. (2011). Landscape hazard assessment in Nain, Phase I: Inventory of surficial sediment types and infrastructure damage, Final Report to Nunatsiavut Government and Nain Inuit Community Government.

Blois, J. L., Williams, J. W., Fitzpatrick, M. C., Jackson, S. T., & Ferrier, S. (2013). Space can substitute for time in predicting climate-change effects on biodiversity. *Proceedings of the National Academy of Sciences*, *110*(23), 9374–9379. https://doi.org/10.1073/pnas.1220228110

Borge, A. F., Westermann, S., Solheim, I., & Etzelmüller, B. (2017). Strong degradation of palsas and peat plateaus in northern Norway during the last 60 years. *The Cryosphere, 11*(1), 1–16. https://doi.org/10.5194/tc-11-1-2017

Borish, D., Cunsolo, A., Snook, J., Shiwak, I., Wood, M., HERD Caribou Project Steering Committee, Mauro, I., Dewey, C., & Harper, S. L. (2021). "Caribou was the reason, and everything else happened after": Effects of caribou declines on Inuit in Labrador, Canada. *Global Environmental Change, 68,* 102268. https://doi.org/10.1016/j.gloenvcha.2021.102268

Bosiö, J., Johansson, M., Callaghan, T. V., Johansen, B., & Christensen, T. R. (2012). Future vegetation changes in thawing subarctic mires and implications for greenhouse gas exchange—A regional assessment. *Climatic Change*, *115*(2), 379–398. https://doi.org/10.1007/s10584-012-0445-1

Brown, R. J. E. (1975). *Permafrost investigations in Quebec and Newfoundland (Labrador)* (p. 99 p.). National Research Council of Canada. https://doi.org/10.4224/20374659

Carpino, O., Haynes, K., Connon, R., Craig, J., Devoie, É., & Quinton, W. (2021). Long-term climate-influenced land cover change in discontinuous permafrost peatland complexes. *Hydrology and Earth System Sciences*, *25*(6), 3301–3317. https://doi.org/10.5194/hess-25-3301-2021

Chasmer, L., & Hopkinson, C. (2017). Threshold loss of discontinuous permafrost and landscape evolution. *Global Change Biology*, *23*(7), 2672–2686. https://doi.org/10.1111/gcb.13537

Christensen, T. R., Johansson, T., Åkerman, H. J., Mastepanov, M., Malmer, N., Friborg, T., Crill, P., & Svensson, B. H. (2004). Thawing sub-arctic permafrost: Effects on vegetation and methane emissions. *Geophysical Research Letters*, *31*(4). https://doi.org/10.1029/2003GL018680

de la Barreda-Bautista, B., Boyd, D. S., Ledger, M., Siewert, M. B., Chandler, C., Bradley, A. V., Gee, D., Large, D. J., Olofsson, J., Sowter, A., & Sjögersten, S. (2022). Towards a Monitoring Approach for Understanding Permafrost Degradation and Linked Subsidence in Arctic Peatlands. *Remote Sensing*, *14*(3), Article 3. https://doi.org/10.3390/rs14030444

Devoie, É. G., Craig, J. R., Dominico, M., Carpino, O., Connon, R. F., Rudy, A. C. A., & Quinton, W. L. (2021). Mechanisms of Discontinuous Permafrost Thaw in Peatlands. Journal of Geophysical Research: Earth Surface, 126(11), e2021JF006204. https://doi.org/10.1029/2021JF006204

Disher, B. S., Connon, R. F., Haynes, K. M., Hopkinson, C., & Quinton, W. L. (2021). The hydrology of treed wetlands in thawing discontinuous permafrost regions. *Ecohydrology*, *14*(5), e2296. https://doi.org/10.1002/eco.2296

Dyke, L. D., & Sladen, W. E. (2010). Permafrost and Peatland Evolution in the Northern Hudson Bay Lowland, Manitoba. *Arctic*, *63*(4), 429–441.

Emmert, A., & Kneisel, C. (2021). Internal structure and palsa development at Orravatnsrústir Palsa Site (Central Iceland), investigated by means of integrated resistivity and ground-penetrating radar methods. *Permafrost and Periglacial Processes*, *32*(3), 503–519. https://doi.org/10.1002/ppp.2106

Errington, R. C., Macdonald, S. E., Melnycky, N. A., & Bhatti, J. S. (2022). Estimating lichen biomass in forests and peatlands of northwestern Canada in a changing climate. Arctic, Antarctic, and Alpine Research, 54(1), 221–238. https://doi.org/10.1080/15230430.2022.2082263

Fewster, R. E., Morris, P. J., Ivanovic, R. F., Swindles, G. T., Peregon, A. M., & Smith, C. J. (2022). Imminent loss of climate space for permafrost peatlands in Europe and Western Siberia. Nature Climate Change, 12(4), Article 4. https://doi.org/10.1038/s41558-022-01296-7

Fillion, M.-È., Bhiry, N., & Touazi, M. (2014). Differential Development of Two Palsa Fields in a Peatland Located near Whapmagoostui-Kuujjuarapik, Northern Québec, Canada. *Arctic, Antarctic, and Alpine Research*, *46*(1), 40–54.

Finnis, J., & Bell, T. (2015). An analysis of recent observed climate trends and variability in Labrador. *Canadian Geographies / Les Géographies Canadiennes*, *59*(2), 151–166. https://doi.org/10.1111/cag.12155

Foster, D. R. and Glaser, P. H. (1986). The raised bogs of southeastern Labrador, Canada: Classification, distribution, vegetation and recent dynamics. *Jounral of Ecology*, 74, 47–71, https://doi.org/10.2307/2260348.

Fraser, R., Lantz, T., Mcfarlane-Winchester, M., van der Sluijs, J., & Prévost, C. (2020). *Testing the potential of UAV photogrammetry for deriving bare earth models in Arctic shrublands.* https://doi.org/10.4095/321447

Grant, R. F., Mekonnen, Z. A., & Riley, W. J. (2019). Modeling Climate Change Impacts on an Arctic Polygonal Tundra: 1. Rates of Permafrost Thaw Depend on Changes in

Vegetation and Drainage. *Journal of Geophysical Research: Biogeosciences*, *124*(5), 1308–1322. https://doi.org/10.1029/2018JG004644

Hagedorn, G. W. (2022). Prelimanry Delineation of Marine Sediments in Eastcentral Labrador: Parts of NTS Map Areas 13F, G, I, J, K, N and O. Current Research, Newfoundland and Labrador Department of Industry, Energy and Technology, 22(1), 189–201.

Hayashi, M., Goeller, N., Quinton, W. L., & Wright, N. (2007). A simple heat-conduction method for simulating the frost-table depth in hydrological models. Hydrological Processes, 21(19), 2610–2622. https://doi.org/10.1002/hyp.6792

Heginbottom. (1995). *Canada, permafrost* [Map]. The Centre.

Hohmann, M. (1997). Soil freezing—The concept of soil water potential. State of the art. *Cold Regions Science and Technology*, *25*(2), 101–110. https://doi.org/10.1016/S0165-232X(96)00019-5

Holloway, J. E., & Lewkowicz, A. G. (2020). Half a century of discontinuous permafrost persistence and degradation in western Canada. *Permafrost and Periglacial Processes*, *31*(1), 85–96. https://doi.org/10.1002/ppp.2017

Hugelius, G., Loisel, J., Chadburn, S., Jackson, R. B., Jones, M., MacDonald, G., Marushchak, M., Olefeldt, D., Packalen, M., Siewert, M. B., Treat, C., Turetsky, M., Voigt, C., & Yu, Z. (2020). Large stocks of peatland carbon and nitrogen are vulnerable to permafrost thaw. *Proceedings of the National Academy of Sciences of the United States of America*, *117*(34), 20438–20446. https://doi.org/10.1073/pnas.1916387117

Istomin, K. V., & Habeck, J. O. (2016). Permafrost and indigenous land use in the northern Urals: Komi and Nenets reindeer husbandry. *Polar Science*, *10*(3), 278–287. https://doi.org/10.1016/j.polar.2016.07.002

James, M., Lewkowicz, A.G., Smith, S.L., and Miceli, C.M. (2013). Multi-decadal degradation and persistence of permafrost in the Alaska Highway corridor, northwest Canada. Environmental Research Letters, 8: 045013. doi:10.1088/1748-9326/8/4/045013.

Jean, M., & Payette, S. (2014a). Dynamics of active layer in wooded palsas of northern Quebec. *Geomorphology*, *206*, 87–96. https://doi.org/10.1016/j.geomorph.2013.10.001

Jean, M., & Payette, S. (2014b). Effect of Vegetation Cover on the Ground Thermal Regime of Wooded and Non-Wooded Palsas. *Permafrost and Periglacial Processes*, *25*(4), 281–294. https://doi.org/10.1002/ppp.1817

Johansson, M., Callaghan, T. V., Bosiö, J., Åkerman, H. J., Jackowicz-Korczynski, M., & Christensen, T. R. (2013). Rapid responses of permafrost and vegetation to experimentally increased snow cover in sub-arctic Sweden. *Environmental Research Letters*, *8*(3), 035025. https://doi.org/10.1088/1748-9326/8/3/035025

Johnson, A., Trant, A., Hermanutz, L., Davis, E., Siegwart Collier, L., Way, R., and Knight, T. (2022). *Tuktu Past, Present, and Future: State of Torngat Mountains Caribou and their Forage in a Changing Environment.* [Master's Dissertation, University of Waterloo]. UWSpace. http://hdl.handle.net/10012/18311

Jones, B. M., Baughman, C. A., Romanovsky, V. E., Parsekian, A. D., Babcock, E. L., Stephani, E., Jones, M. C., Grosse, G., Berg, E. E., Kanevskiy, M., & Kääb, A. (2016). Presence of rapidly degrading permafrost plateaus in south-central Alaska. Cryosphere, 10(6), 2673–2692. https://doi.org/10.5194/tc-10-2673-2016

Karger, D. N., Conrad, O., Böhner, J., Kawohl, T., Kreft, H., Soria-Auza, R. W., Zimmermann, N. E., Linder, H. P., and Kessler, M. (2017). Climatologies at high resolution or the earth's land surface areas, *Scientific Data*, 4, 170122, https://doi.org/10.1038/sdata.2017.122.

Karger, D. N., Conrad, O., Böhner, J., Kawohl, T., Kreft, H., Soria-Auza, R. W., Zimmermann, N. E., Linder, H. P., and Kessler, M. (2018) Climatologies at high resolution for the earth's land surface areas V2.1. *EnviDat* [data set], https://doi.org/10.16904/envidat.228.v2.1.

Karjalainen, O., Luoto, M., Aalto, J., Etzelmüller, B., Grosse, G., Jones, B. M., Lilleøren, K. S., & Hjort, J. (2020). High potential for loss of permafrost landforms in a changing climate. *Environmental Research Letters*, *15*(10), 104065. https://doi.org/10.1088/1748-9326/abafd5

Keuper, F., Dorrepaal, E., van Bodegom, P. M., van Logtestijn, R., Venhuizen, G., van Hal, J., & Aerts, R. (2017). Experimentally increased nutrient availability at the permafrost thaw front selectively enhances biomass production of deep-rooting subarctic peatland species. *Global Change Biology*, *23*(10), 4257–4266. https://doi.org/10.1111/gcb.13804

Lewkowicz, A. G., Etzelmüller, B., & Smith, S. L. (2011). Characteristics of Discontinuous Permafrost based on Ground Temperature Measurements and Electrical Resistivity Tomography, Southern Yukon, Canada. *Permafrost and Periglacial Processes*, *22*(4), 320–342. https://doi.org/10.1002/ppp.703

Luoto, M., & Seppala, M. (2003). Thermokarst ponds as indicators of the former distribution of palsas in Finnish Lapland. *Permafrost and Periglacial Processes*, *14*(1), 19–27. https://doi.org/10.1002/ppp.441

Mamet, S. D., Chun, K. P., Kershaw, G. G. L., Loranty, M. M., & Peter Kershaw, G. (2017). Recent Increases in Permafrost Thaw Rates and Areal Loss of Palsas in the

Western Northwest Territories, Canada. *Permafrost and Periglacial Processes*, *28*(4), 619–633. https://doi.org/10.1002/ppp.1951

Markkula, I., Turunen, M., & Rasmus, S. (2019). A review of climate change impacts on the ecosystem services in the Saami Homeland in Finland. *Science of The Total Environment*, *692*, 1070–1085. https://doi.org/10.1016/j.scitotenv.2019.07.272

McGarigal, K., & Marks, B. J. (1995). FRAGSTATS: Spatial pattern analysis program for quantifying landscape structure. (PNW-GTR-351; p. PNW-GTR-351). U.S. Department of Agriculture, Forest Service, Pacific Northwest Research Station. https://doi.org/10.2737/PNW-GTR-351

Norton, C. H., Cuerrier, A., & Hermanutz, L. (2021). People and Plants in Nunatsiavut (Labrador, Canada): Examining Plants as a Foundational Aspect of Culture in the Subarctic. *Economic Botany*, *75*(3/4), 287–301. https://doi.org/10.1007/s12231-021-09530-7

O'Neill, H. B., Wolfe, S. A., & Duchesne, C. (2019). New ground ice maps for Canada using a paleogeographic modelling approach. The Cryosphere, 13(3), 753–773. https://doi.org/10.5194/tc-13-753-2019

Payette, S., Delwaide, A., Caccianiga, M., & Beauchemin, M. (2004). Accelerated thawing of subarctic peatland permafrost over the last 50 years. *Geophysical Research Letters*, *31*(18). https://doi.org/10.1029/2004GL020358

Peppin, S. S. L., & Style, R. W. (2013). The Physics of Frost Heave and Ice-Lens Growth. *Vadose Zone Journal*, *12*(1), vzj2012.0049. https://doi.org/10.2136/vzj2012.0049

Pironkova, Z. (2017). Mapping Palsa and Peat Plateau Changes in the Hudson Bay Lowlands, Canada, Using Historical Aerial Photography and High-Resolution Satellite Imagery. *Canadian Journal of Remote Sensing*, *43*(5), 455–467. https://doi.org/10.1080/07038992.2017.1370366

Rivas, C. A., Guerrero-Casado, J., & Navarro-Cerrillo, R. M. (2022). A New Combined Index to Assess the Fragmentation Status of a Forest Patch Based on Its Size, Shape Complexity, and Isolation. *Diversity*, *14*(11), 896. https://doi.org/10.3390/d14110896

Roberts, B. A., Simon, N. P. P., and Deering, K. W. (2006). The forests and woodlands of Labrador, Canada: Ecology, distribution and future management. *Ecological Research*, 21, 868–880, https://doi.org/10.1007/s11284-006-0051-7, 2006.

Seppälä, M. (2011). Synthesis of studies of palsa formation underlining the importance of local environmental and physical characteristics. *Quaternary Research*, *75*(2), 366–370. https://doi.org/10.1016/j.yqres.2010.09.007

Schmelzer, I., Lewis, K. P., Jacobs, J. D., & McCarthy, S. C. (2020). Boreal caribou survival in a warming climate, Labrador, Canada 1996–2014. *Global Ecology and Conservation*, *23*, e01038. https://doi.org/10.1016/j.gecco.2020.e01038

Shur, Y. L., & Jorgenson, M. T. (2007). Patterns of permafrost formation and degradation in relation to climate and ecosystems. *Permafrost and Periglacial Processes*, *18*(1), 7–19. https://doi.org/10.1002/ppp.582

Schuur, E. G., McGuire, A. D., Schadel, C., Grosse, G., Harden, J. W., Hayes, D. J., Hugelius, G., Koven, C. D., Kuhry, P., Lawrence, D. M., Natali, S. M., Olefeldt, D., Romanovsky, V. E., Schaefer, K., Turetsky, M. R., Treat, C. C., & Vonk, J. E. (2015). Climate change and the permafrost carbon feedback. Nature, 520(7546), 171–180. https://doi.org/10.1038/nature14338

Smith, M. W., & Riseborough, D. W. (2002). Climate and the limits of permafrost: A zonal analysis. *Permafrost and Periglacial Processes*, *13*(1), 1–15. https://doi.org/10.1002/ppp.410

Smith, S. L., O'Neill, H. B., Isaksen, K., Noetzli, J., & Romanovsky, V. E. (2022). The changing thermal state of permafrost. *Nature Reviews Earth & Environment*, *3*, 10–23. https://doi.org/10.1038/ s43017-021-00240-1

Sollid, J. L., & Sorbel, L. (1998). Palsa bogs as a climate indicator; examples from Dovrefjell, Southern Norway. *Ambio*, *27*(4), 287–291.

Tarnocai, C., Canadell, J. G., Schuur, E. a. G., Kuhry, P., Mazhitova, G., & Zimov, S. (2009). Soil organic carbon pools in the northern circumpolar permafrost region. *Global Biogeochemical Cycles*, *23*(2). https://doi.org/10.1029/2008GB003327

Van der Sluijs, J., Kokelj, S. V., Fraser, R. H., Tunnicliffe, J., & Lacelle, D. (2018). Permafrost Terrain Dynamics and Infrastructure Impacts Revealed by UAV Photogrammetry and Thermal Imaging. *Remote Sensing*, *10*(11), Article 11. https://doi.org/10.3390/rs10111734

Verdonen, M., Störmer, A., Lotsari, E., Korpelainen, P., Burkhard, B., Colpaert, A., & Kumpula, T. (2023). Permafrost degradation at two monitored palsa mires in north-west Finland. *The Cryosphere*, *17*(5), 1803–1819. https://doi.org/10.5194/tc-17-1803-2023

Wang, Y., Way, R. G., Beer, J., Forget, A., Tutton, R., & Purcell, M. C. (2023). Significant underestimation of peatland permafrost along the Labrador Sea coastline in northern Canada. *The Cryosphere*, *17*(1), 63–78. https://doi.org/10.5194/tc-17-63-2023

Wang, Y., Way, R.G., & Beer, J. (in press). Multi-decadal degradation and fragmentation of palsas and peat plateaus in coastal Labrador, northeastern Canada. *Environmental Research Letters*.

Ward, L. M., Hill, M. J., Antane, N., Chreim, S., Olsen Harper, A., & Wells, S. (2021). "The Land Nurtures Our Spirit": Understanding the Role of the Land in Labrador

Innu Wellbeing. *International Journal of Environmental Research and Public Health*, *18*(10), Article 10. https://doi.org/10.3390/ijerph18105102

Way, R. G., Lewkowicz, A. G., & Bonnaventure, P. P. (2017). Development of moderate-resolution gridded monthly air temperature and degree-day maps for the Labrador-Ungava region of northern Canada. *International Journal of Climatology*, *37*(1), 493–508. https://doi.org/10.1002/joc.4721

Way, R. G., Lewkowicz, A. G., & Zhang, Y. (2018). Characteristics and fate of isolated permafrost patches in coastal Labrador, Canada. *The Cryosphere*, *12*(8), 2667–2688. https://doi.org/10.5194/tc-12-2667-2018

Westoby, M. J., Brasington, J., Glasser, N. F., Hambrey, M. J., & Reynolds, J. M. (2012). 'Structure-from-Motion' photogrammetry: A low-cost, effective tool for geoscience applications. *Geomorphology*, *179*, 300–314. https://doi.org/10.1016/j.geomorph.2012.08.021

Zoltai, S. C., & Tarnocai, C. (1971). Properties of a Wooded Palsa in Northern Manitoba. *Arctic and Alpine Research*, *3*(2), 115–129. https://doi.org/10.2307/1549981

Supplemental material for "Uncrewed aerial vehicle-based assessments of peatland permafrost resiliency along the Labrador Sea coastline, northern Canada"

[1]Beer, J., [1]Wang, Y., [1]Way, R., [1]Forget, A., & [1]Colyn, V.

[1]Northern Environmental Geosciences Laboratory, Queen's University, Kingston, Ontario, Canada

S1 - Site Photos

Photos taken at ground level in 2021 or 2022 are provided for all twenty study sites.

Figure S1. Site photo of NA1 taken in 2022.

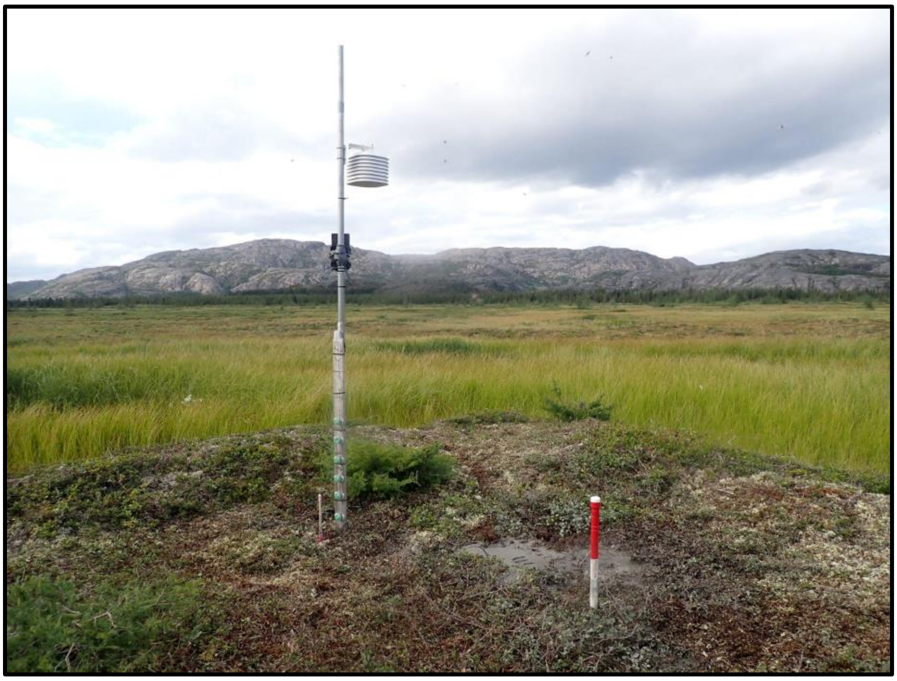

Figure S2. Site photo of NA2 taken in 2022.

Figure S3. Site photo of RG1 taken in 2021.

Figure S4. Site photo of RG2 taken in 2021.

Figure S5. Site photo of RG3 taken in 2022.

Figure S6. Site photo of RG4 taken in 2022.

Figure S7. Site photo of CW1 taken in 2021.

Figure S8. Site photo of CW2 taken in 2021.

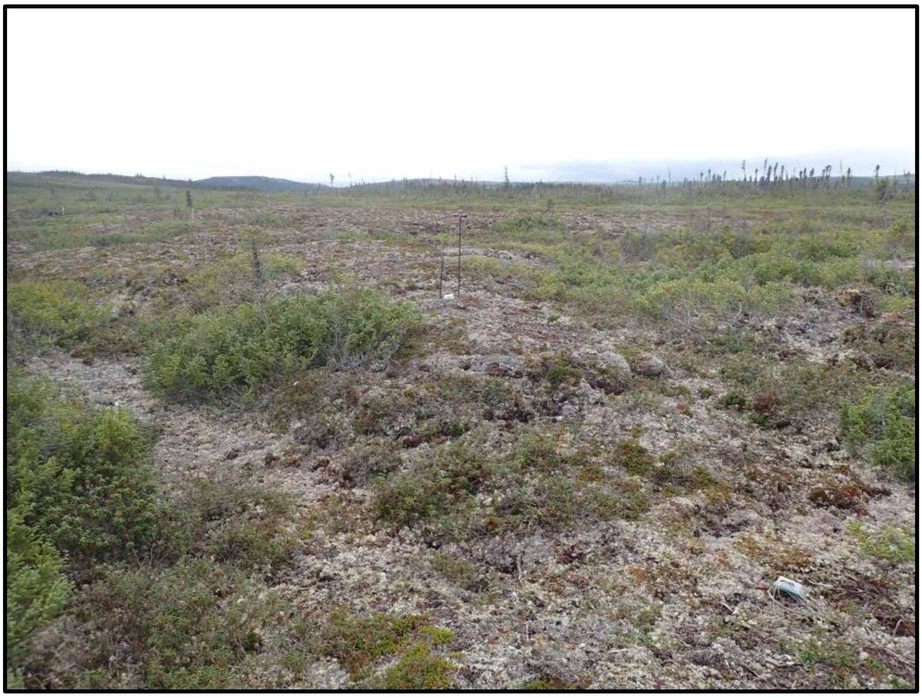

Figure S9. Site photo of CW3 taken in 2021.

Figure S10. Site photo of CW4 taken in 2022.

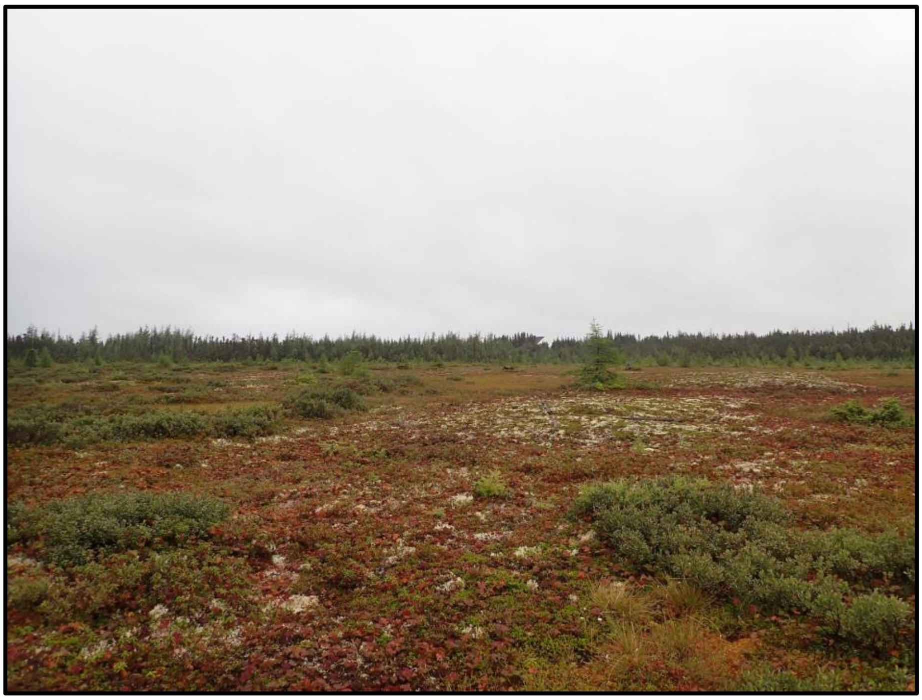

Figure S11. Site photo of CW5 taken in 2021

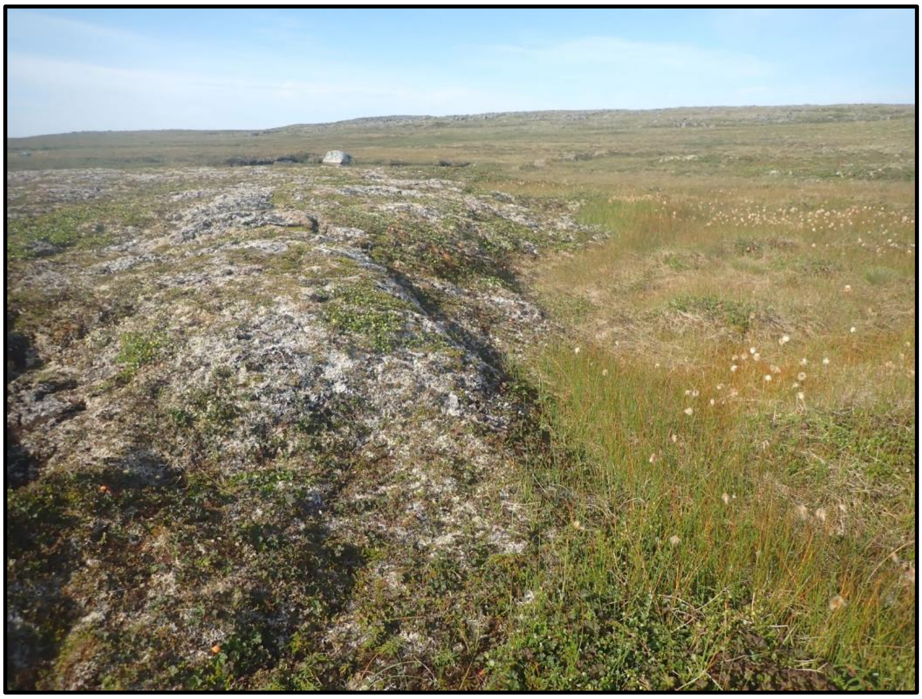

Figure S12. Site photo of BT1 taken in 2022.

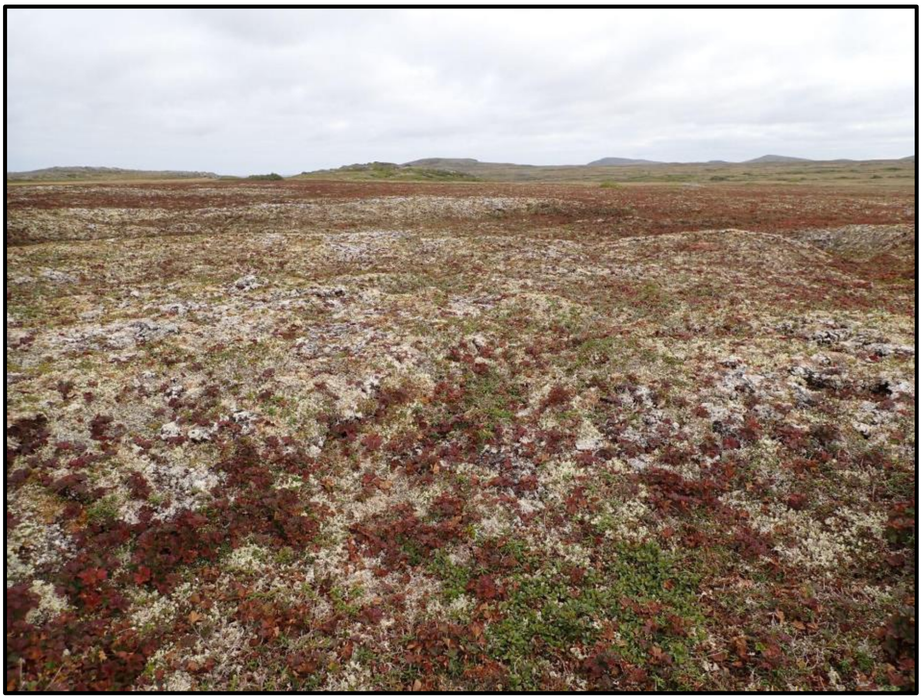

Figure S13. Site photo of BT2 taken in 2021.

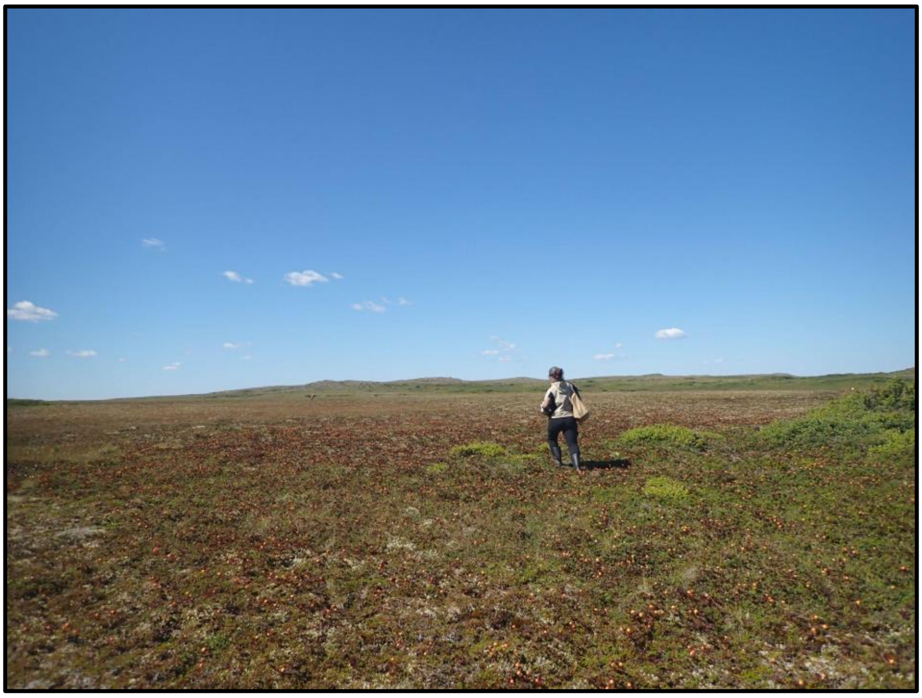

Figure S14. Site photo of BT3 taken in 2022.

Figure S15. Site photo of BT4 taken in 2022.

Figure S16. Site photo of RB1 taken in 2021.

Figure S17. Site photo of RB2 taken in 2021

Figure S18. Site photo of RB3 taken in 2022.

Figure S19. Site photo of RB4 taken in 2021.

Figure S20. Site photo of BS1 taken in 2021.

S2 - Orthomosaics and peatland permafrost tracings

Orthomosaics for all twenty sites visited in this study. Traced polygons show the boundaries of permafrost mounds and are superimposed on site Orthomosaics. The thick black lines show the boundary of the bog within each survey, excluding some areas near survey edges where data was sparse. Differently coloured polygons are solely used to simplify visualization, and do not reflect differences in data or processing. Superimposed points show confirmed presence (blue) or absence (red) of frozen ground from frost probing or temperature profiles.

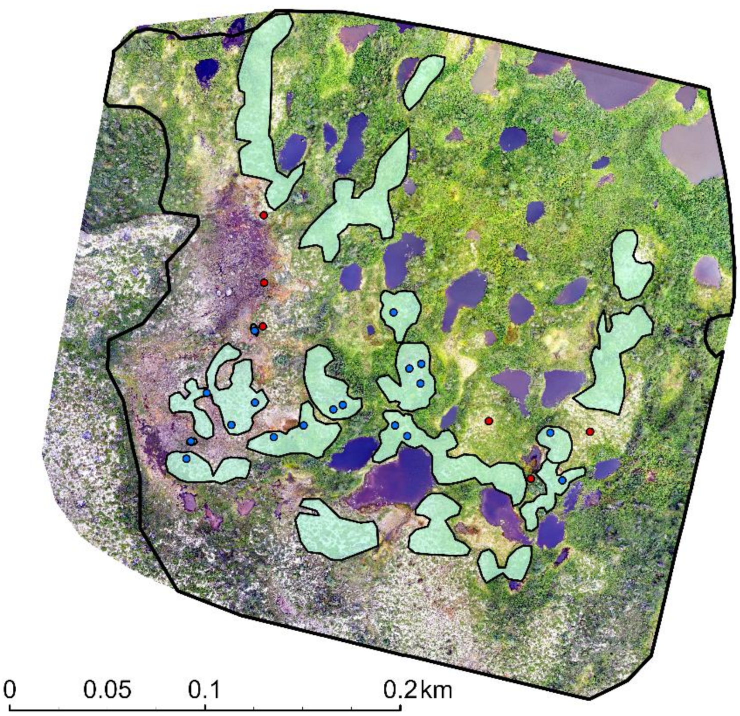

Figure S21. Orthomosaic of NA1 with overlain peatland permafrost tracings.

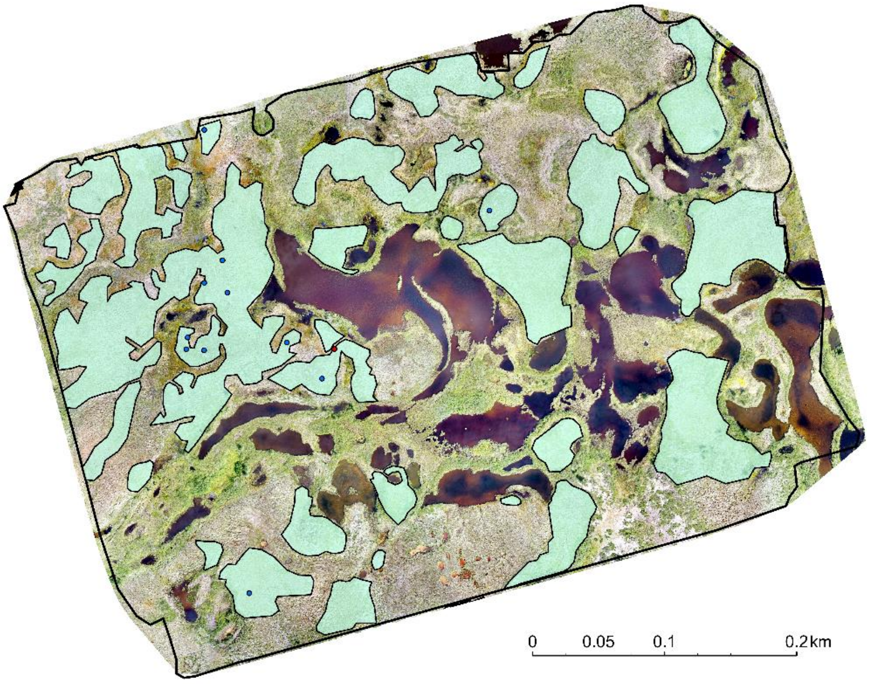

1031 Figure S22. Orthomosaic of NA2 with overlain peatland permafrost tracings.

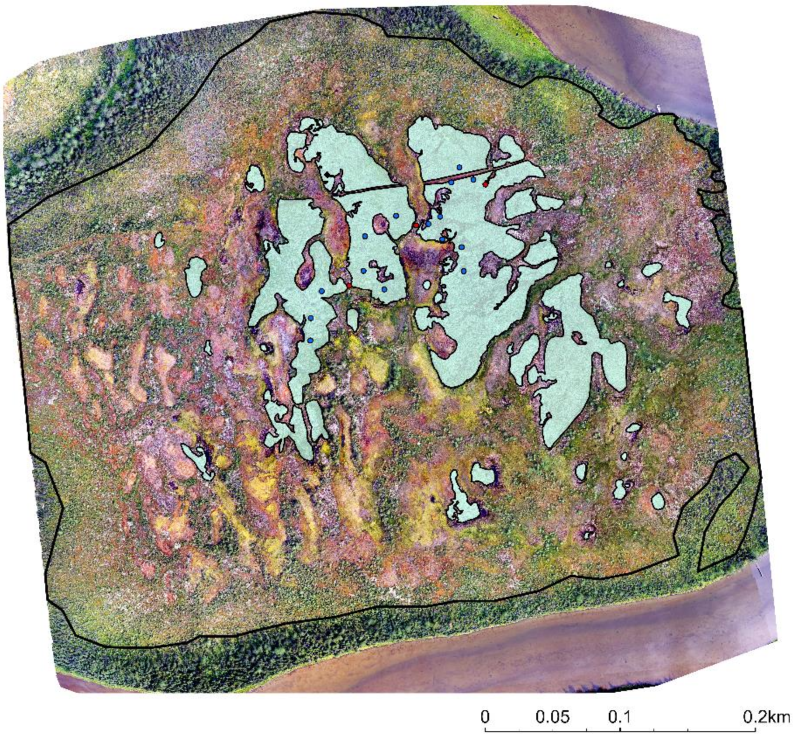

1032 Figure S23. Orthomosaic of RG1 with overlain peatland permafrost tracings.

1033

1034

1035

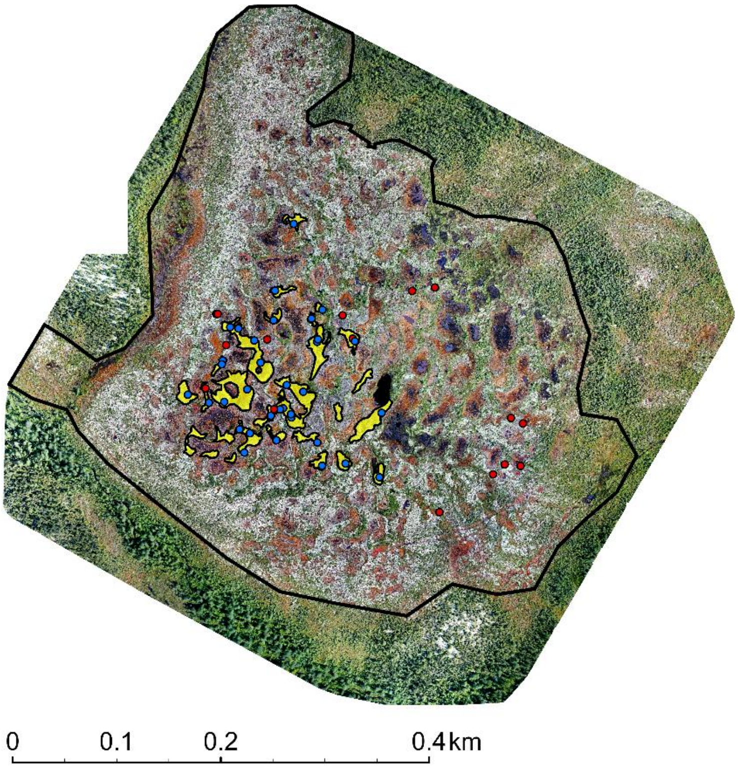

Figure S24. Orthomosaic of RG2 with overlain peatland permafrost tracings.

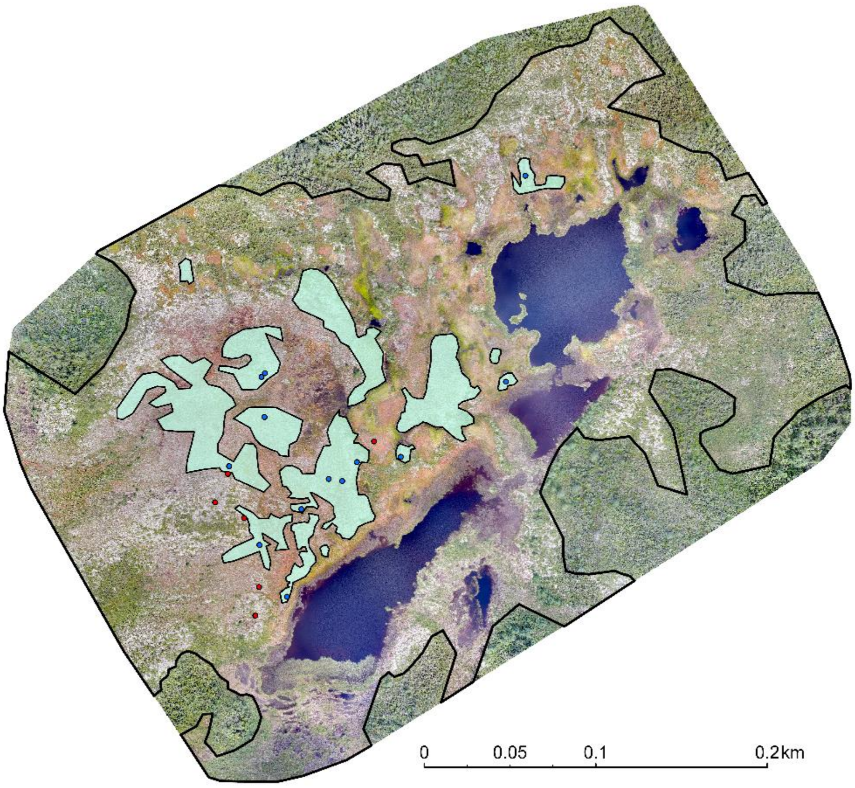

Figure S25. Orthomosaic of RG3 with overlain peatland permafrost tracings.

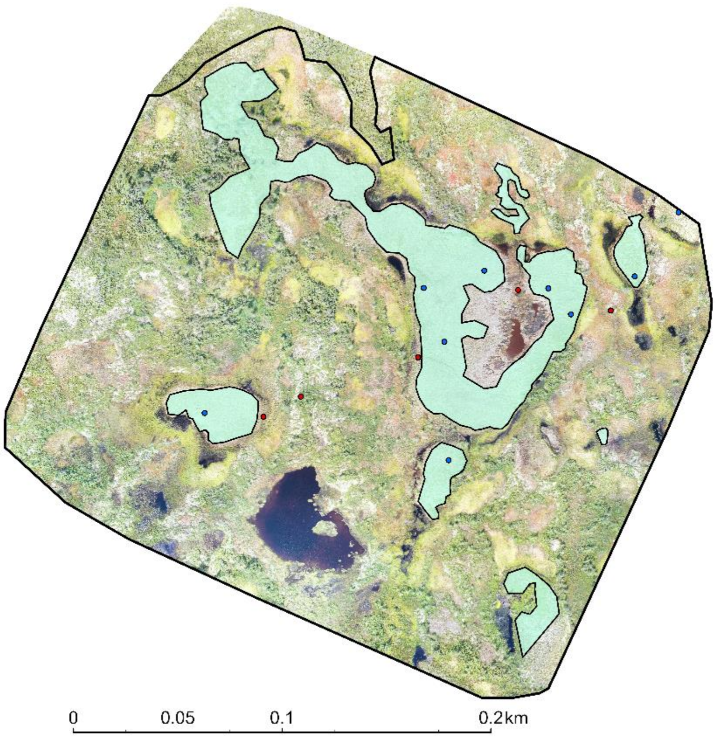

Figure S26. Orthomosaic of RG4 with overlain peatland permafrost tracings.

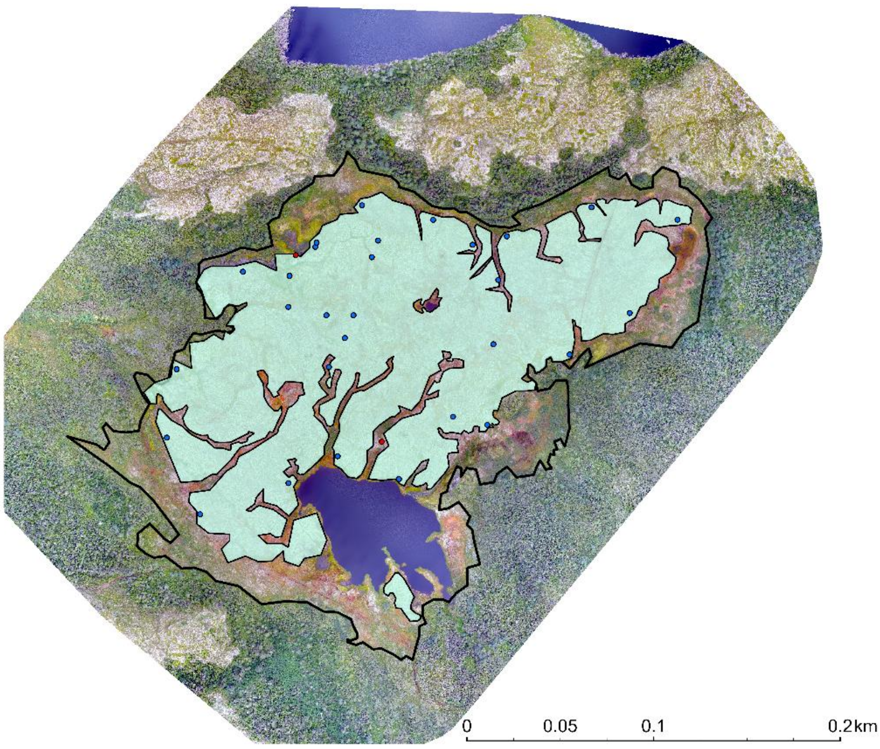

Figure S27. Orthomosaic of CW1 with overlain peatland permafrost tracings.

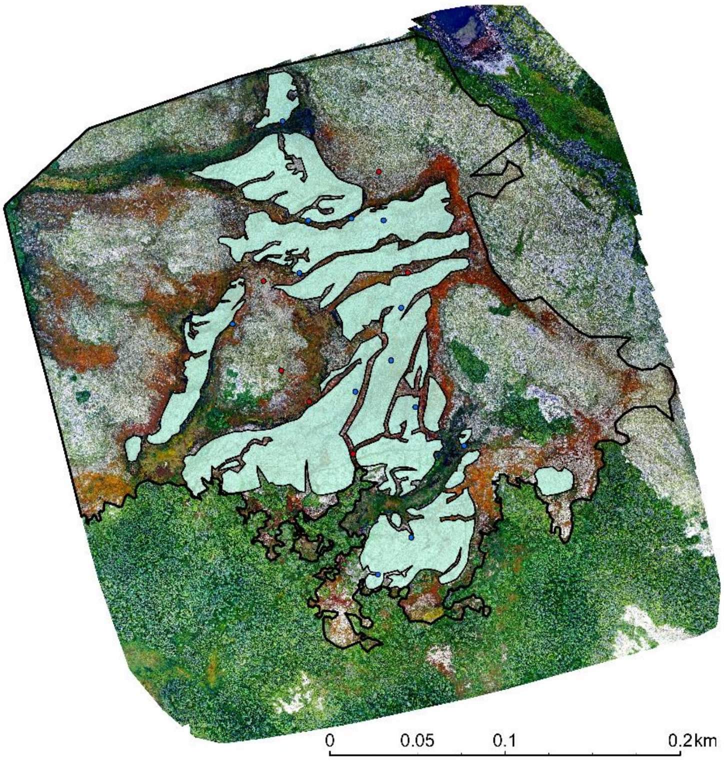

Figure S28. Orthomosaic of CW2 with overlain peatland permafrost tracings.

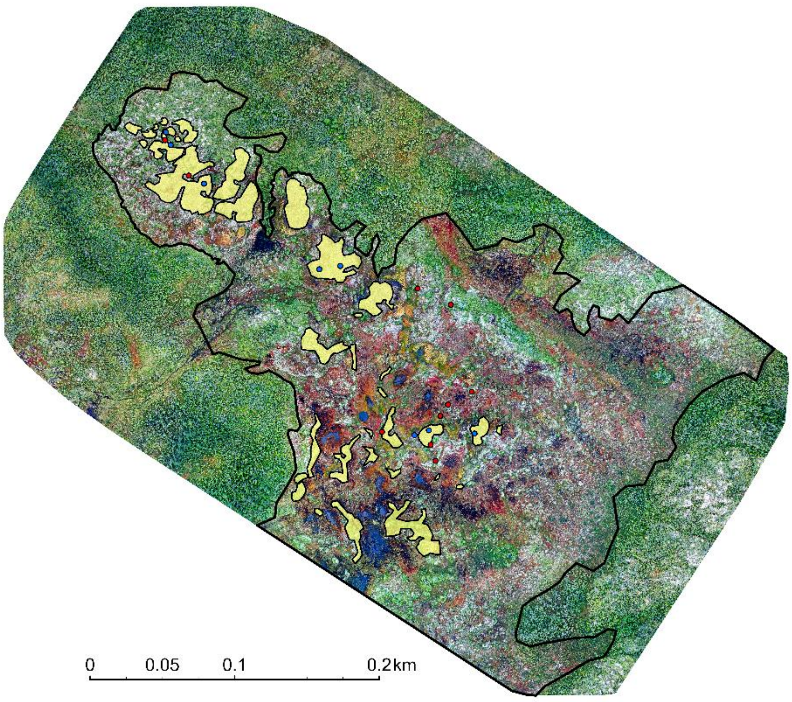

Figure S29. Orthomosaic of CW3 with overlain peatland permafrost tracings.

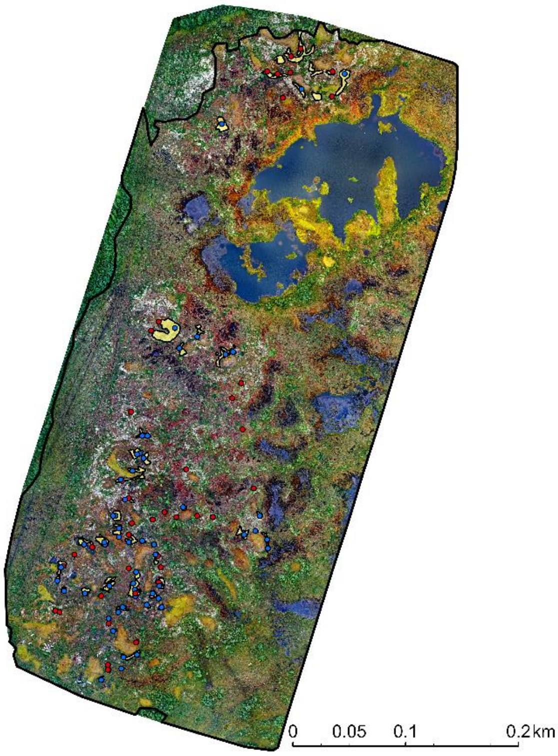

Figure S30. Orthomosaic of CW4 with overlain peatland permafrost tracings.

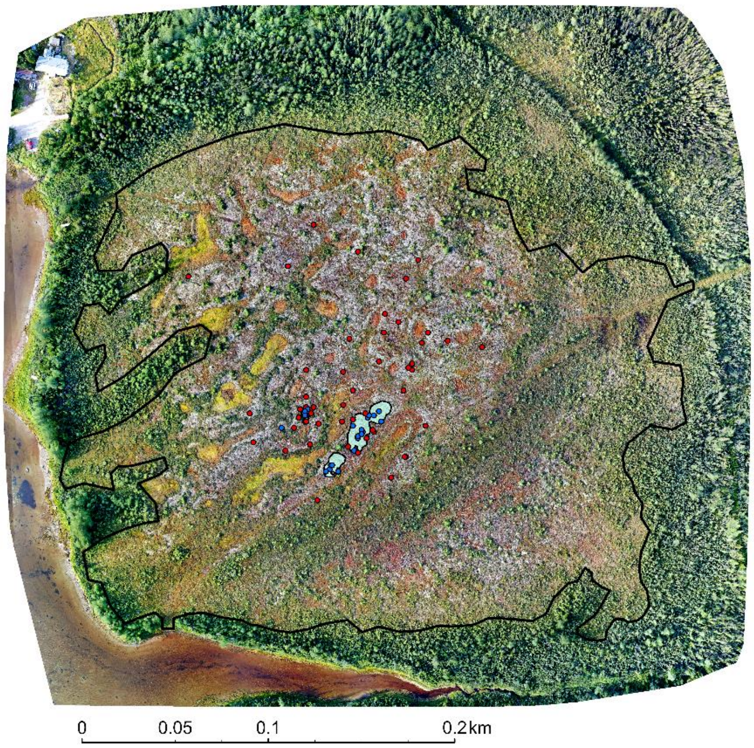

Figure S31. Orthomosaic of CW5 with overlain peatland permafrost tracings.

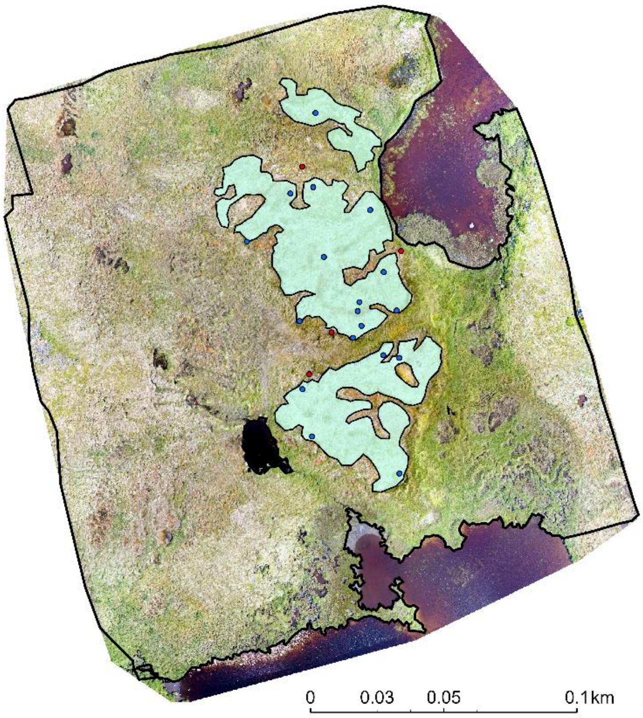

Figure S32. Orthomosaic of BT1 with overlain peatland permafrost tracings

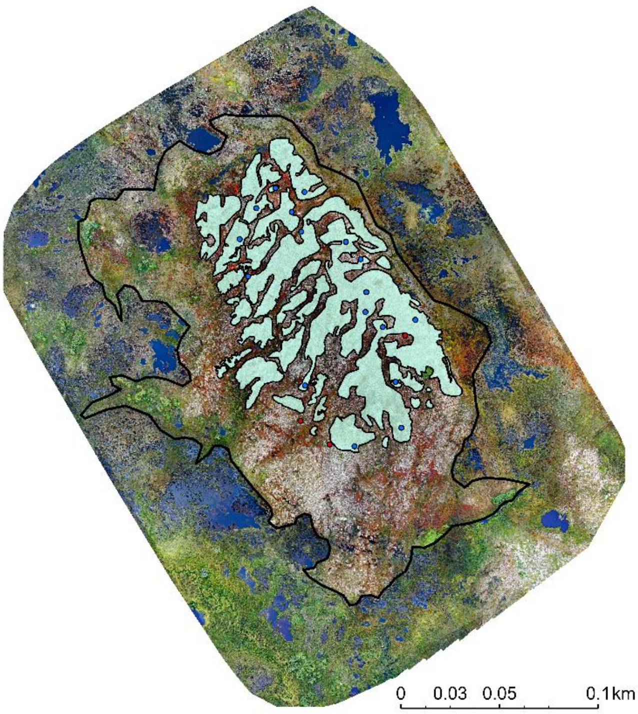

Figure S33. Orthomosaic of BT2 with overlain peatland permafrost tracings

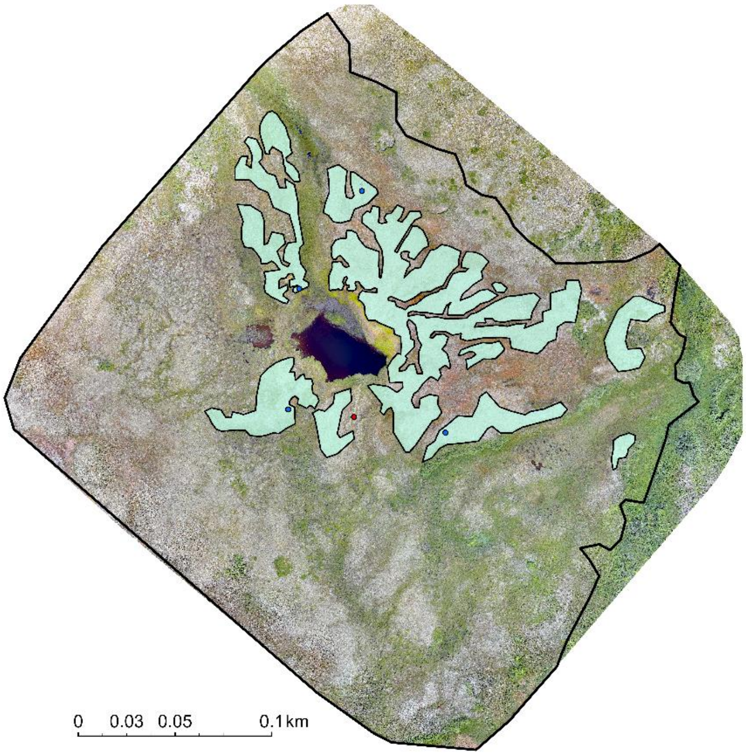

Figure S34. Orthomosaic of BT3 with overlain peatland permafrost tracings

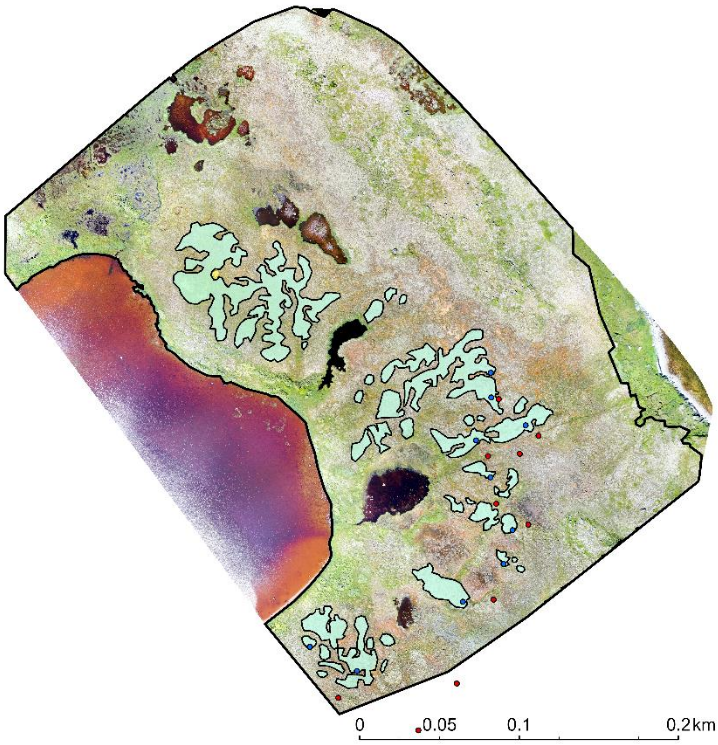

Figure S35. Orthomosaic of BT4 with overlain peatland permafrost tracings

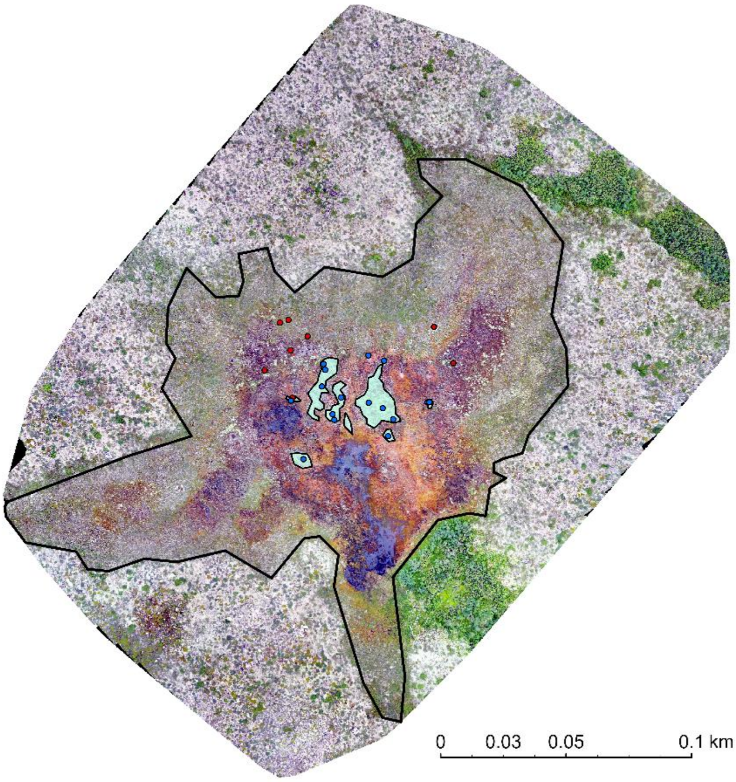

Figure S36. Orthomosaic of RB1 with overlain peatland permafrost tracing

Figure S37. Orthomosaic of RB2 with overlain peatland permafrost tracings

Figure S38. Orthomosaic of RB3 with overlain peatland permafrost tracings

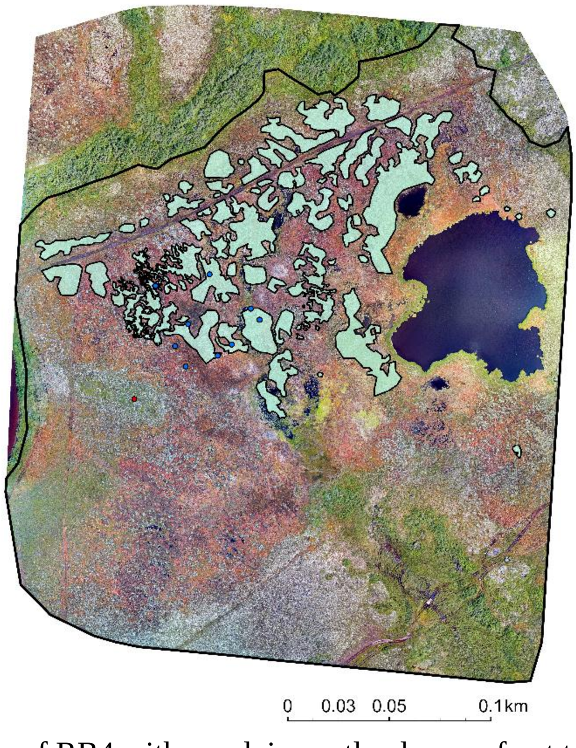

Figure S39. Orthomosaic of RB4 with overlain peatland permafrost tracings

1071 Figure S40. Orthomosaic of BS1 with overlain peatland permafrost tracings

1072

1073

1074 S3- Digital workflow

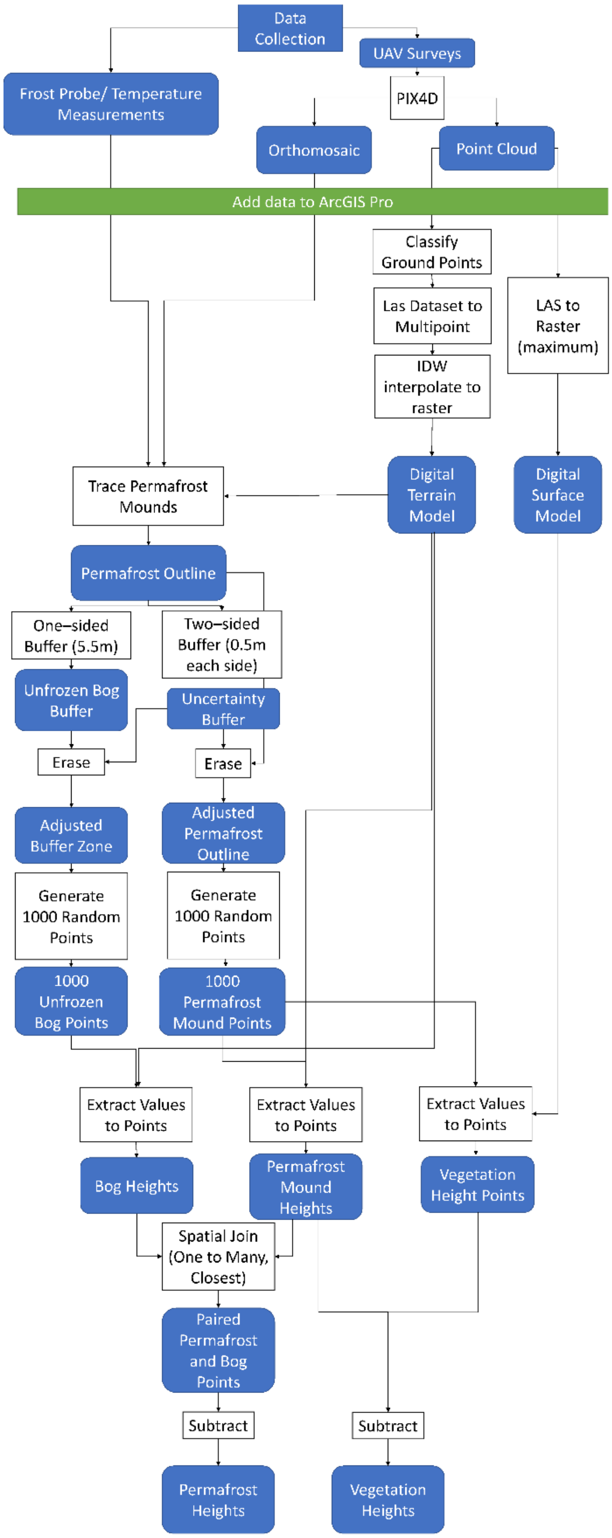

1075

1076 Figure S41. Diagram showing workflow for digital processing steps used in this study. White
1077 boxes represent digital processing steps, while blue boxes represent raw or processed data.